

**DOKUZ EYLÜL UNIVERSITY**  
**GRADUATE SCHOOL OF NATURAL AND APPLIED SCIENCES**

**POSITIONING OF RADIO SOURCES VIA  
ESTIMATION OF DIRECTION OF ARRIVAL**

**by**  
**Serkan KOCA**

**January, 2015**  
**İZMİR**

# **POSITIONING OF RADIO SOURCES VIA ESTIMATION OF DIRECTION OF ARRIVAL**

**A Thesis Submitted to the  
Graduate School of Natural And Applied Sciences of Dokuz Eylül University  
In Partial Fulfillment of the Requirements for the Degree of Master of Science in  
Electrical and Electronics Engineering Program**

**by  
Serkan KOCA**

**January, 2015**


**İZMİR**

**M.Sc THESIS EXAMINATION RESULT FORM**

We have read the thesis entitled "**POSITIONING OF RADIO SOURCES VIA ESTIMATION OF DIRECTION OF ARRIVAL**" completed by **SERKAN KOCA** under supervision of **ASST. PROF. DR. SERKAN GÜNEL** and we certify that in our opinion it is fully adequate, in scope and in quality, as a thesis for the degree of Master of Science.

  
.....  
Asst. Prof. Dr. Serkan GÜNEL

Supervisor

  
.....  
Assoc. Prof. Dr. Olcay Akay

Jury Member

  
.....  
Assoc. Prof. Dr. Hacer ÖZÜNK

Jury Member

  
.....  
Prof. Dr. Ayşe OKUR

Director

Graduate School of Natural and Applied Sciences

## **ACKNOWLEDGEMENTS**

I would like to express my special appreciation and thanks to my supervisor Asst. Prof. Dr. Serkan GÜNEL, you have been a tremendous mentor for me. I would like to thank you for encouraging my research and for allowing me to grow as a research scientist. Your advice on both research as well as on my career have been priceless.

A special thanks to my family. Words cannot express how grateful I am to my mother and father for all of the sacrifices that you've made on my behalf. Your prayer for me was what sustained me thus far. I would also like to thank all of my friends who supported me in writing, and incited me to strive towards my goal.

Serkan KOCA

# **POSITIONING OF RADIO SOURCES VIA ESTIMATION OF DIRECTION OF ARRIVAL**

## **ABSTRACT**

Positioning of a radio source is the estimation of location of the radio source in three dimensional (3-D) space with respect to a reference point. A system, based on positioning of radio sources can be used for pedestrian or vehicle tracking and navigation. The direction of arrival estimation of a signal emitted by a radio source can be used to estimate the location of the radio source. An antenna array system enables the direction of arrival estimation with proper array signal processing methods. The multiple signal classification (MUSIC) algorithm has been the most widely used method that estimates the direction of arrival of a signal received by a uniform linear array antenna system. The estimation of the azimuth and the elevation angles of a signal can be used to determine the position of the signal source in 3-D space with respect to the spherical coordinate system. The main goal of this study is to design an active system that simultaneously determines the position of multiple radio sources via the estimation of direction of arrival. A Matlab<sup>TM</sup> based simulation software has been developed to examine performance of the active radio source positioning system.

**Keywords:** Radio sources, positioning, direction of arrival estimation, multiple signal classification algorithm, antenna array systems

# **GELİŞ YÖNÜ KESTİRİMİ İLE RADYO KAYNAKLARININ KONUMUNUN BELİRLENMESİ**

## **ÖZ**

Radyo kaynaklarının konumlandırılması konumu bilinmeyen radyo kaynaklarının bir referans noktasına göre üç boyutlu uzayda konumunun kestirilmesidir. Radyo kaynaklarının konumunun belirlenmesine dayalı bir sistem yaya veya araç takibi ve navigasyonu için kullanılabilir. Radyo kaynaklarından yayılan sinyallerin geliş yönünün kestirilmesi radyo kaynağının konumunun kestirilmesinde kullanılabilir. Anten dizi sistemi uygun dizi sinyal işleme yöntemleri ile geliş yönünün kestirilmesini mümkün kılmaktadır. Düzgün dağılımlı doğrusal anten dizileri ile sinyalin geliş yönünün kestirimini yapan çoklu sinyal sınıflandırma algoritması en yaygın kullanılan yöntemdir. Sinyal kaynağının azimut ve yükselti açılarının kestirilmesi üç boyutlu uzayda küresel koordinatlara göre konumunun belirlenmesi için kullanılabilir. Bu çalışmanın temel amacı geliş yönü kestirimi ile çoklu radyo kaynaklarının eş zamanlı konumlandırmasını yapan aktif sistemin tasarımıdır. Radyo kaynakları konumlandırma aktif sisteminin performansının incelenebilmesi için Matlab<sup>TM</sup> tabanlı benzetim programı geliştirilmiştir.

**Anahtar kelimeler:** Radyo kaynakları, konumlandırma, geliş yönü kestirimi, çoklu sinyal sınıflandırma algoritması, anten dizi sistemleri

## CONTENTS

	Page
THESIS EXAMINATION RESULT FORM.....	ii
ACKNOWLEDGEMENTS.....	iii
ABSTRACT.....	iv
ÖZ.....	v
LIST OF FIGURES.....	ix
LIST OF TABLES.....	x
 CHAPTER ONE – INTRODUCTION.....	 1
 CHAPTER TWO – QUADRATURE AMPLITUDE MODULATION.....	 7
2.1 Amplitude Modulation.....	7
2.1.1 Double-Sideband AM.....	7
2.1.2 Demodulation of DSB Amplitude Modulation.....	8
2.2 Quadrature Amplitude Modulation.....	10
2.2.1 Demodulation of QAM.....	11
 CHAPTER THREE – DIRECTION OF ARRIVAL ESTIMATION.....	 14
3.1 Model of Array Observation.....	15
3.1.1 Uniform Linear Array System.....	16
3.2 Amplitude Modulated Signal Received by ULA.....	17
3.3 Multiple Signal Classification.....	19
 CHAPTER FOUR – POSITION ESTIMATION.....	 23
4.1 Coordinate Systems and Transformations.....	23
4.1.1 Coordinate Systems.....	23
4.1.2 Affine Transformation.....	24
4.1.2.1 Translation.....	25

4.1.2.2 Rotation	26
4.1.2.3 Combination of Rotation and Translation Matrix	29
4.2 Positioning	30
4.2.1 Positioning via Direction of Arrival	32
<b>CHAPTER FIVE – HARDWARE DESIGN</b>	<b>36</b>
5.1 Inset Fed Microstrip Patch Antenna Design	38
5.1.1 2.41 GHz Inset Fed Microstrip Patch Antenna Design	40
5.1.2 Inset-Fed Microstrip Patch Antenna Array	48
5.2 Chebyshev Bandpass Filter Design	51
5.3 RF Driver Amplifier Design	53
5.3.1 RF Driver Amplifier with Bandpass Filter	54
5.4 Low Noise Amplifier Design	56
5.4.1 Low Noise Amplifier with Bandpass Filter	58
<b>CHAPTER SIX – SIMULATIONS AND PERFORMANCE ASSESSMENT</b>	<b>60</b>
6.1 Trajectory Tracking	65
<b>CHAPTER SEVEN – CONCLUSION</b>	<b>68</b>
<b>REFERENCES</b>	<b>70</b>



## LIST OF FIGURES

	Page
Figure 1.1 Conceptual design of radio source positioning .....	4
Figure 1.2 Block diagram of positioning system.....	5
Figure 2.1 Block diagram of DSB AM modulator.....	7
Figure 2.2 DSB AM signal in the time domain.....	8
Figure 2.3 Frequency spectrum of DSB AM signal.....	9
Figure 2.4 Block diagram of DSB AM demodulator.....	9
Figure 2.5 Quadrature amplitude modulation and demodulation.....	11
Figure 2.6 QAM signal in the time domain.....	12
Figure 3.1 The DoA estimation problem.....	14
Figure 3.2 Array system geometry.....	15
Figure 3.3 Uniform Linear Array antenna system.....	17
Figure 3.4 Power spectrum of MUSIC function.....	21
Figure 3.5 Power spectrum of MUSIC function w.r.t. AM signals.....	22
Figure 4.1 Coordinate system and basis vectors.....	23
Figure 4.2 Translation of a point.....	26
Figure 4.3 Rotation about the $x$ axes.....	27
Figure 4.4 Rotation about the $y$ axes.....	28
Figure 4.5 Rotation about the $z$ axes.....	28
Figure 4.6 Affine transformation and combination of rotation and translation.....	29
Figure 4.7 Representation of a point with respect to reference coordinate system.....	31
Figure 4.8 The positioning of a point represented in spherical coordinate notation.....	33
Figure 5.1 The hardware design of the radio source positioning system.....	37
Figure 5.2 The inset-fed microstrip patch antenna geometry.....	38
Figure 5.3 The inset-fed patch antenna ANSYS HFSS 3D Model.....	41
Figure 5.4 The minimum VSWR versus inset-fed length.....	43
Figure 5.5 The minimum $S_{11}$ S-parameter versus inset-fed length.....	43
Figure 5.6 The minimum $S_{11}$ of the patch antenna versus frequency.....	44

Figure 5.7 The VSWR of patch antenna versus frequency.....	45
Figure 5.8 The $S_{11}$ parameter of patch antenna versus frequency .....	45
Figure 5.9 The radiation pattern of the patch antenna .....	47
Figure 5.10 The inset-fed micristripped patch antenna array .....	49
Figure 5.11 The radiation pattern of the patch antenna .....	50
Figure 5.12 The S-parameters of the antenna array system .....	51
Figure 5.13 The 3 <sup>rd</sup> order Chebyshev bandpass filter .....	51
Figure 5.14 The frequency response of the Chebyshev bandpass filter .....	52
Figure 5.15 The schematic of the RF driver amplifier design .....	53
Figure 5.16 The S-parameters of the RF driver amplifier .....	54
Figure 5.17 The GP, GA and GT of the amplifier w.r.t. frequency .....	55
Figure 5.18 The frequency response of the RF driver amplifier with bandpass filter .....	55
Figure 5.19 The GP, GA and GT of the combined system .....	56
Figure 5.20 The schematic of the low noise amplifier design .....	57
Figure 5.21 The frequency response of the low noise amplifier .....	57
Figure 5.22 The GP, GA and GT of the low noise amplifier .....	58
Figure 5.23 The frequency response of the low noise amplifier with bandpass filter .....	59
Figure 5.24 The GP, GA and GT of the combined system .....	59
Figure 6.1 The position estimation error versus SNR .....	61
Figure 6.2 The position estimation error versus SNR .....	62
Figure 6.3 The position estimation error versus carrier frequency .....	64
Figure 6.4 The trajectory tracking with positioning system .....	65
Figure 6.5 The trajectory tracking with positioning system .....	67

## LIST OF TABLES

	Page
Table 5.1 The basic parameters of patch antenna design.....	41
Table 5.2 The basic antenna parameters obtained by HFSS.....	45
Table 5.3 The electrical properties of the inset-fed patch antenna.....	46
Table 5.4 The electrical properties of the patch antenna array.....	48
Table 5.5 The values of the lumped components of the designed bandpass filter.....	52
Table 6.1 The position estimation error versus SNR.....	61
Table 6.2 The position estimation error versus signal to noise ratio.....	62
Table 6.3 The position estimation error versus carrier frequency.....	64
Table 6.4 The trajectory tracking with positioning system.....	66
Table 6.5 The trajectory tracking with positioning system.....	67

## CHAPTER ONE

### INTRODUCTION

Positioning of a radio source is estimation of location of the radio source in three dimensional (3-D) space with respect to a reference point. A system, based on positioning of radio sources can be used for pedestrian or vehicle tracking and navigation. Time of Flight (ToF) / Time of Arrival (ToA), Time Difference of Arrival (TDoA) and Received Signal Strength Indication (RSSI) are available methods and techniques that enable positioning. The ToF/ToA measures time of flight of a signal that travels from signal source (transmitter) to receiver. Relation between speed of signal and ToF can be used to calculate the distance between transmitter and receiver on ToF/ToA based positioning systems (Lanzisera et al., 2011). The TDoA describes time differences of arrival of signals emitted from different transmitters. The measured TDoA from two transmitters defines a hyperbolic curve and intersection of curves gives location of receiver or navigator (Gustafsson & Gunnarsson, 2003). The RSSI estimates distances between transmitter and receivers using received signal strength. The estimated distances are used with trilateration algorithm to calculate the position of transmitters (Oguejiofor et al., 2013). There are a few existing systems providing positioning such as Global Positioning System (GPS) and Long Range Navigation (LORAN) system.

The GPS is a satellite based navigation system that can be used to locate positions. The GPS satellites, which are equipped with atomic clocks, transmits radio signals that contain their exact location, time and other information. The receiver uses ToF or ToA to calculate distance from each satellite and uses trilateration method to determine position. The system needs at least four or more satellites to calculate the accurate 3-D position (Zarchan, 1996). Although it is possible to locate positions with sub-centimeter accuracy in GPS, the information is scrambled so that it provides 3 meters accuracy for commercial applications.

LORAN is a pulsed medium-frequency long-range hyperbolic navigation system and is based on time difference of arrival (TDoA). LORAN system is developed in

World War II for navigating ships and aircrafts. A pair of LORAN transmitters emit a pulse simultaneously. The navigator uses TDoA of received pulses to calculate differences between the distances traveled by the pulses. Intersections represent a pair of measured time differences and define a point that is the location of navigator. In LORAN, each TDoA value is measured with accuracy of about 100 nanoseconds which corresponds to about 30 meters accuracy for localization. LORAN needs at least four stations and their position information to determine position in 2-D.

Positioning systems can be separated into two groups; passive and active systems. In passive positioning systems, mobile receiver uses signals which are emitted from stationary transmitters and their location information to calculate its position. Inversely, the receivers are mobile and the transmitters are stationary in active systems. The stationary receivers calculate position of mobile transmitters using signals emitted by transmitter. The active systems are inefficient when very large distances are measured. Because, the mobile transmitters need more power to reach signals to stationary receivers. In this sense, GPS and LORAN are passive systems. However, they are inefficient for short ranged accurate positioning due to extremely precious timing requirements.

Another method that can be used for estimating the location of a radio source is Direction of Arrival (DoA) estimation. This technique consists of estimating angle of arrival of a signal radiated by the source using antenna. The DoA estimations and triangulation method can be used together to determine position of a signal source. Accurate estimation of signal DoA is important in communication and radar systems including sonar, radio astronomy, seismology, navigation and surveillance systems (Hwang et al., 2008; Evans et al., 1982). Use of a single antenna to estimate signal DoA restricts performance and accuracy of estimation, since antenna main lobe and beamwidth are inversely proportional to antenna physical size. Instead of using a single antenna, utilization of an antenna array and efficient signal processing methods increase performance and accuracy of DoA estimation (Lee et al., 2005).

Antenna array systems are formed by antennas distributed in space. They are widely used in communication and radar systems to enable manipulation of received signals for enhancement and parameter estimation (Godara, 1997a). They help to reduce cochannel interference, system complexity and cost, bit error rate and outage probability by using array processing methods such as conventional, null-steering, adaptive beam forming (Rappaport, 1991; Godara, 1997b). The received data at different antenna elements on array are phase shifted according to signals DoA and the position of the antenna elements in space and there is one-to-one relationship between the direction of incoming signal and received signal data on each element. This relationship is inverted by array signal processing techniques to determine signal DoA. The DoA can be determined by spectral estimation methods that determine local maximums which are DoA of signals in spatial spectrum (Johnson, 1982), Maximum likelihood estimation that maximizes log-likelihood function of received signal data to determine signal DoA (El-Beheri & MacPhie, 1977; Miller & Fuhrmann, 1990), Estimation of Signal Parameters via Rotational Invariance Techniques (ESPRIT) algorithm (Roy & Kailath, 1989) and Multiple Signal Classification (MUSIC) algorithm (Hwang et al., 2008; Schmidt, 1986; Barabell, 1983).

Multiple Signal Classification (MUSIC) Algorithm has been widely used method to estimate direction of signals. The MUSIC algorithm provides unbiased estimation of; the number of the signals, direction of arrival, the polarization of signal, the noise power and amount of interference (Schmidt, 1986). There are four basic algorithms based on MUSIC to estimate DoA. These are:

- *Spectral MUSIC*; is simple and effective eigenstructure based DoA estimation method. It is a widely studied method and has many variations (Schmidt, 1986).
- *Root MUSIC*; is only used with uniformly distributed antenna arrays to estimate DoA. DoA estimation in this case, is based on determination of roots of polynomials. Root MUSIC algorithm has better performance than Spectral MUSIC method (Barabell, 1983).

- *Constrained MUSIC*; erases components of known signal sources parameters from data matrix to improve DoA estimation of unknown sources. Then, updated matrix is used to determine direction of unknown sources (DeGroat et al., 1993).
- *Beam-Space MUSIC*; applies beam-forming techniques before application of any of MUSIC algorithms for DoA estimation method. The Beam-Space DoA estimation advantages are decreasing computational costs, improved resolution, decreasing sensitivity against system errors (Mayhan & Niro, 1987; Zoltowski et al., 1993b,a).

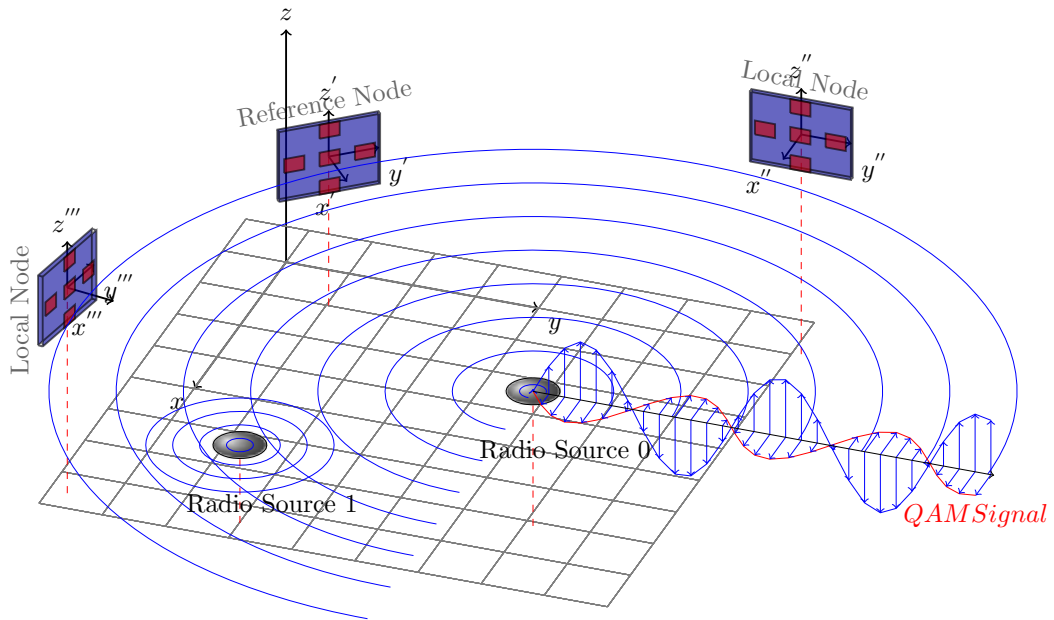


Figure 1.1 Conceptual design of radio source positioning

The main goal of this study is to design a system that simultaneously determines the position of multiple radio sources, produce and emit quadrature amplitude modulated (QAM) signals (William & Lajos, 1994), in three dimensional space via estimation of direction of arrival. For this purpose, the spectral MUSIC algorithm has been used with Uniform Linear Array (ULA) antenna to obtain DoA angles (azimuth and elevation) to locate the active radio sources in 3-D space. The ULA are formed by antennas oriented along a line in space with uniform spacing. Two ULA antenna arrays have been oriented along y and z axis to obtain the azimuth and the elevation angles and

broadside of ULA antenna arrays are oriented along x axis on a reference or local node as shown in Figure (1.1). The radio sources have active role during positioning process. The design of radio sources has been done to lower cost and to decrease physical size. Hence, the ULA antenna system has been designed using microstrip patch antennas that receive analog QAM signals. Also, the positioning system overall cost has been decreased by use of QAM. The rotation and translation properties of the coordinate transformations have been used to solve the 3-D positioning problem with obtained azimuth and elevation angles. The positioning problem has been reduced to solution of a system of linear equations. A Matlab<sup>TM</sup> based simulation software has been developed to examine performance of overall system.

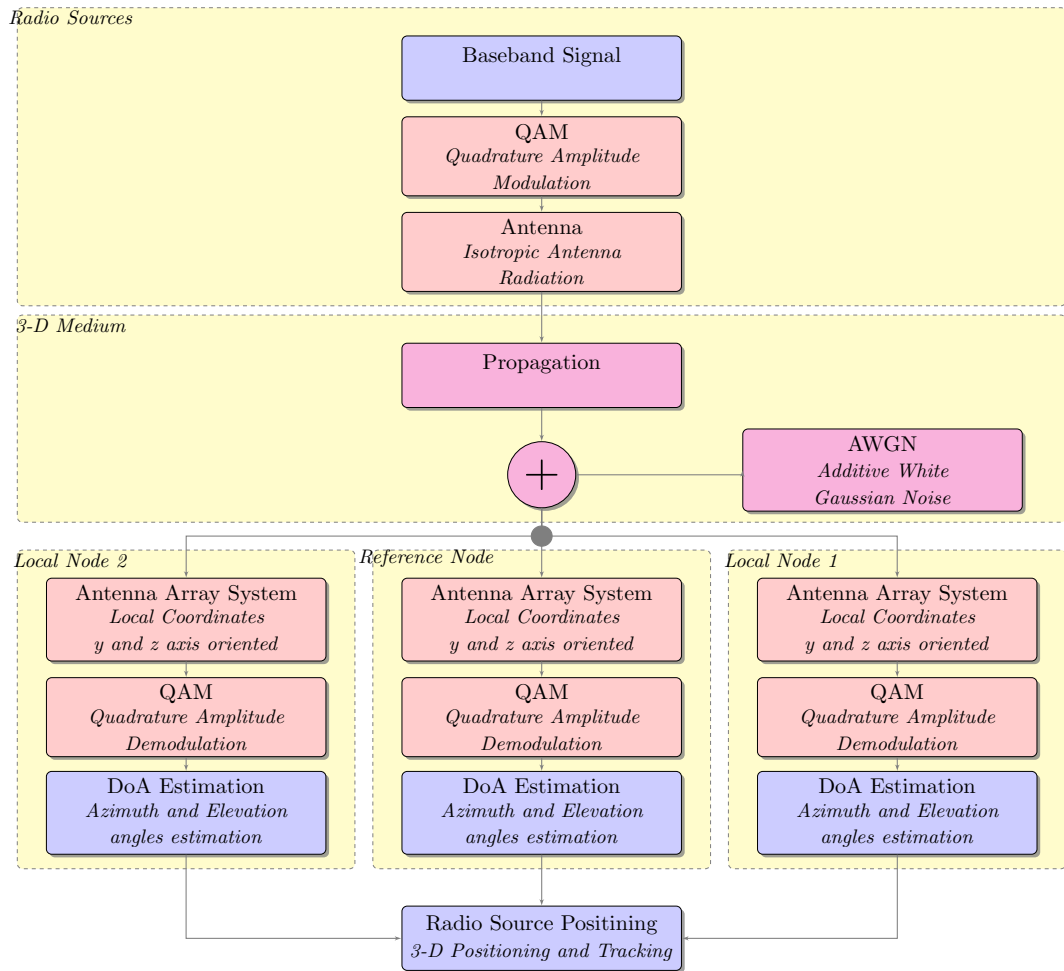


Figure 1.2 Block diagram of positioning system

The block diagram of the radio source positioning system has been shown in Figure (1.2). Initially, a baseband signal is modulated using analog QAM technique in



radio source whose position to be determined. Then, the modulated signal radiates and propagates through medium in 3-D space and arrives at antenna array system on reference node and local nodes. Each antenna element on the array system receives the impinging signal which is time delayed (or phase shifted) at different antenna elements related to signal direction of arrival. The received signal is demodulated to obtain phase shifted baseband signal. To obtain the azimuth and the elevation angles, the spectral MUSIC algorithm is used. Finally, system of linear equations is solved to obtain the position of the radio source in 3-D space.

## CHAPTER TWO

### QUADRATURE AMPLITUDE MODULATION

#### 2.1 Amplitude Modulation

Amplitude Modulation (AM) is a modulation technique used in electronic communication, most commonly for transmitting information via a radio carrier wave. The AM works by varying the strength (amplitude) of transmit signal in relation to the information being sent.

##### 2.1.1 Double-Sideband AM

A Double-Sideband (DSB) AM signal is obtained by multiplying the message signal  $m(t)$  which consists of dc offset with the carrier signal  $c(t)$ . Thus, we have the DSB AM signal,

$$u(t) = [1 + m(t)]c(t) \quad (2.1)$$

where the message signal is constrained to satisfy the condition that  $|m(t)| \leq 1$ .

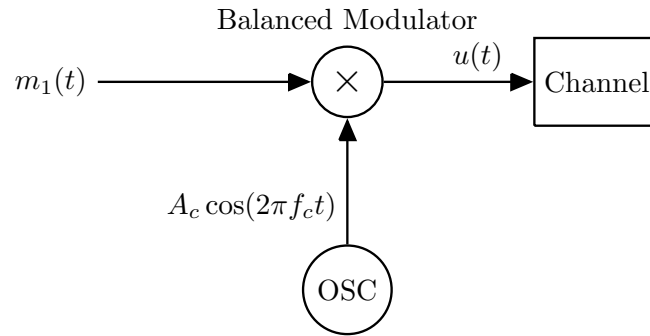


Figure 2.1 Block diagram of DSB AM modulator

Suppose that the carrier wave  $c(t)$  is modeled as a sinusoidal wave,

$$c(t) = A_c \cos(\omega_c t + \phi_c), \quad (2.2)$$

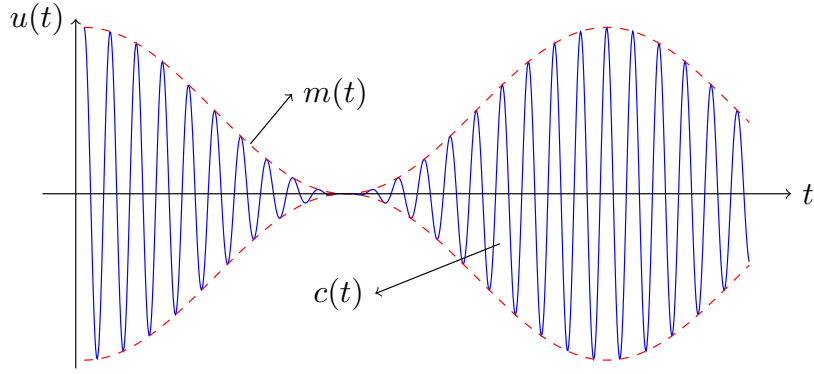


Figure 2.2 DSB AM signal in the time domain

where  $A_c$  carrier amplitude,  $\omega_c$  angular frequency and  $\phi_c$  phase of carrier signal. Let  $m(t)$  represent the message signal to be transmitted,

$$m(t) = A_m \cos(\omega_m t + \phi_m) \quad (2.3)$$

it is assumed that  $\omega_m \ll \omega_c$  and that  $\min[m(t)] = -A_m$ . Amplitude modulation is formed by product,

$$\begin{aligned} u(t) &= [1 + m(t)]c(t) \\ &= [1 + A_m \cos(\omega_m t + \phi_m)]A_c \cos(\omega_c t + \phi_c) \end{aligned} \quad (2.4)$$

The AM modulation index is the measure of amplitude variation surrounding an unmodulated carrier. It is defined as  $h = A_m/A_c$ . We can expand Equation (2.4) and assume that modulation index is 100% ( $A_c = 1$  and  $A_m = 1$ ):

$$u(t) = \cos(\omega_c t + \phi_c) + \cos(\omega_m t + \phi_m) \cos(\omega_c t + \phi_c) \quad (2.5)$$

By using trigonometric identities, we can rewrite Equation (2.5):

$$u(t) = \cos(\omega_c t + \phi_c) + \frac{1}{2} [\cos((\omega_c - \omega_m)t + \phi_c - \phi_m) + \cos((\omega_c + \omega_m)t + \phi_c + \phi_m)] \quad (2.6)$$

The modulated signal has three components: a carrier wave and two sinusoidal waves (known as sidebands), whose frequencies are slightly above and below  $\omega_c$ . The frequency spectrum of AM signal is in Figure (2.3).

### 2.1.2 Demodulation of DSB Amplitude Modulation

There are two types of DSB AM demodulator, envelope and product detector. The envelope detector is simplest way which consists of a diode and RC circuit. The

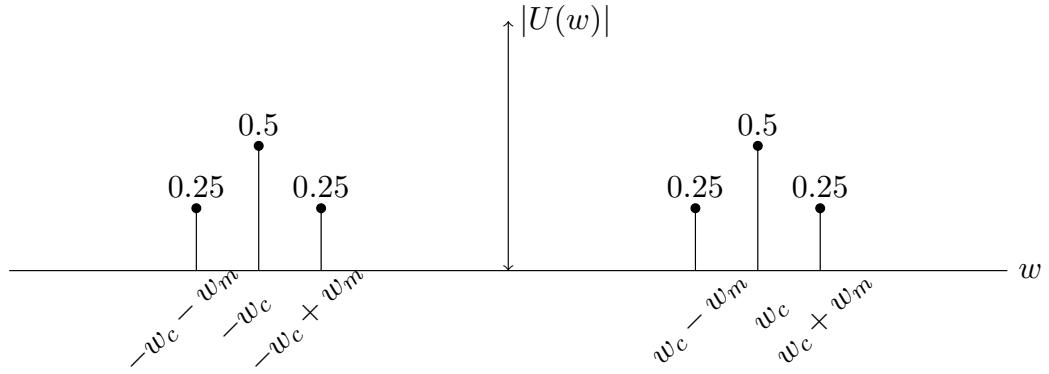


Figure 2.3 Frequency spectrum of DSB AM signal

product detector has better quality but has additional circuit complexity. It takes product of the AM signal and the local oscillator.

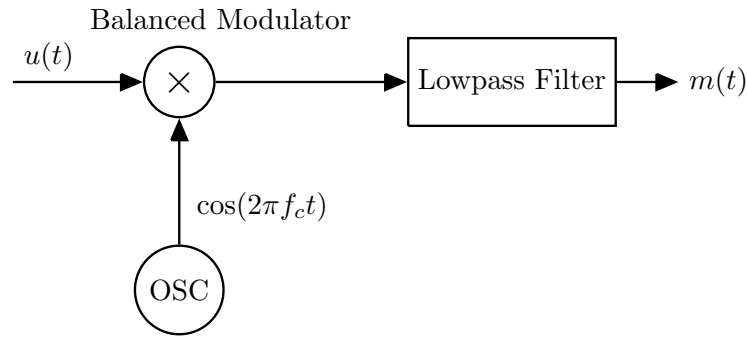


Figure 2.4 Block diagram of DSB AM demodulator

Let  $u(t)$  be AM signal with modulation index is 100% and  $\phi_c, \phi_m$  are zero:

$$u(t) = [1 + \cos(\omega_m t)] \cos(\omega_c t) \quad (2.7)$$

It is assumed that local oscillator is a sinusoidal wave  $\cos(\omega_c t + \phi_r)$  which has same angular frequency with carrier signal and random phase  $\phi_r$ . Demodulated signal is:

$$\tilde{u}(t) = [1 + \cos(\omega_m t)] \cos(\omega_c t) \cos(\omega_c t + \phi_r) \quad (2.8)$$

By using trigonometric identities;

$$\begin{aligned} \tilde{u}(t) &= [1 + \cos(\omega_m t)] \frac{1}{2} [\cos(\phi_r) + \cos(2\omega_c t + \phi_r)] \\ &= \frac{1}{2} [\cos(\phi_r) + \cos(2\omega_c t + \phi_r) + \cos(\omega_m t) \cos(\phi_r) + \cos(\omega_m t) \cos(2\omega_c t + \phi_r)] \end{aligned} \quad (2.9)$$

By filtering out the high frequency components and the DC component, the message signal is obtained,

$$\tilde{m}(t) = \frac{1}{2} \cos(\phi_r) \cos(\omega_m t) \quad (2.10)$$

The message signal is attenuated by the factor  $\cos(\phi_r)$ . A Phase Locked Loop (PLL) can be used to eliminate the attenuation factor by removing the phase difference between local oscillator and received signal. Also, the frequency of the local oscillator must be same with the frequency of the carrier signal.

## 2.2 Quadrature Amplitude Modulation

Quadrature Amplitude Modulation is a type of signal multiplexing method, also known as Quadrature-Carrier Multiplexing. It describes both an analog and a digital modulation scheme for analog and digital communication systems (John & Masoud, 2002). It allows to transmit two message signals on the same carrier frequency, using two quadrature carriers  $A_c \cos(2\pi f_c t)$  and  $A_c \sin(2\pi f_c t)$ . Suppose that  $m_1(t)$  and  $m_2(t)$  are two message signals to be transmitted over channel. The signal  $m_1(t)$  modulates the carrier  $A_c \cos(2\pi f_c t)$  and the signal  $m_2(t)$  modulates the quadrature carrier  $A_c \sin(2\pi f_c t)$ . The two modulated signals are added and transmitted over the channel. Hence, the transmitted signal is

$$u_{QAM}(t) = A_c m_1(t) \cos(2\pi f_c t) + A_c m_2(t) \sin(2\pi f_c t) \quad (2.11)$$

Basically, the two message signals are modulated and transmitted by Double-Sideband Amplitude Modulation (DSB AM) (William & Lajos, 1994). The QAM modulation and demodulation scheme is shown on Figure (2.5).

Suppose that message signals  $m_1(t)$  and  $m_2(t)$  real and imaginary part of complex baseband signal,

$$e^{j\omega_0 t} = \cos(\omega_0 t) + j \sin(\omega_0 t) \quad (2.12)$$

where  $\omega_0$  angular frequency of complex baseband signal. The message signals,

$$m_1(t) = 1 + \cos(\omega_0 t), \quad (2.13)$$

$$m_2(t) = 1 + \sin(\omega_0 t) \quad (2.14)$$

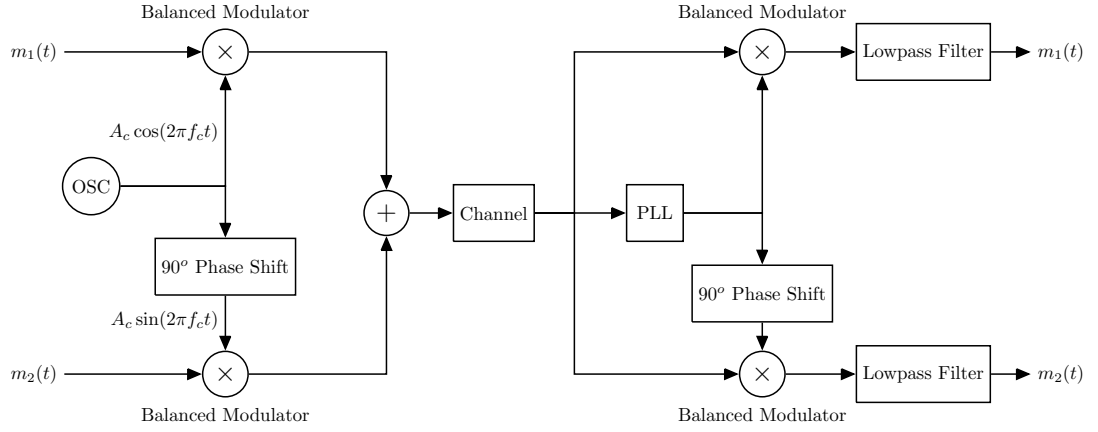


Figure 2.5 Quadrature amplitude modulation and demodulation scheme

The QAM signal is obtained by inserting (2.13) and (2.14) into (2.11) (assume  $A_c = 1$ ),

$$\begin{aligned} u_{QAM}(t) &= [1 + \cos(\omega_0 t)] \cos(\omega_c t) + [1 + \sin(\omega_0 t)] \sin(\omega_c t) \\ &= \cos(\omega_c t) + \cos(\omega_0 t) \cos(\omega_c t) + \sin(\omega_c t) + \sin(\omega_0 t) \sin(\omega_c t) \end{aligned} \quad (2.15)$$

Using trigonometric identities, we can simplify (2.15),

$$u_{QAM}(t) = \cos(\omega_c t) + \sin(\omega_c t) + \cos((\omega_c - \omega_0)t) \quad (2.16)$$

### 2.2.1 Demodulation of QAM

To recover the message signals  $m_1(t)$  and  $m_2(t)$  in received QAM signal  $u_{QAM}(t)$ , the synchronous demodulator is required. That is, the demodulator must use a coherent phase reference, which is usually generated by means of a Phase-Locked Loop (PLL) to demodulate the received signal. The general configuration of the QAM demodulator is shown in Figure (2.5). A PLL is used to generate a phase-coherent carrier signal. The carrier signal and its quadrature which is  $90^\circ$  phase shifted are mixed with received signal  $u_{QAM}(t)$  in balanced modulators. The output of the balanced modulators are passed through a lowpass filter and baseband message signals  $m_1(t)$  and  $m_2(t)$  are recovered.

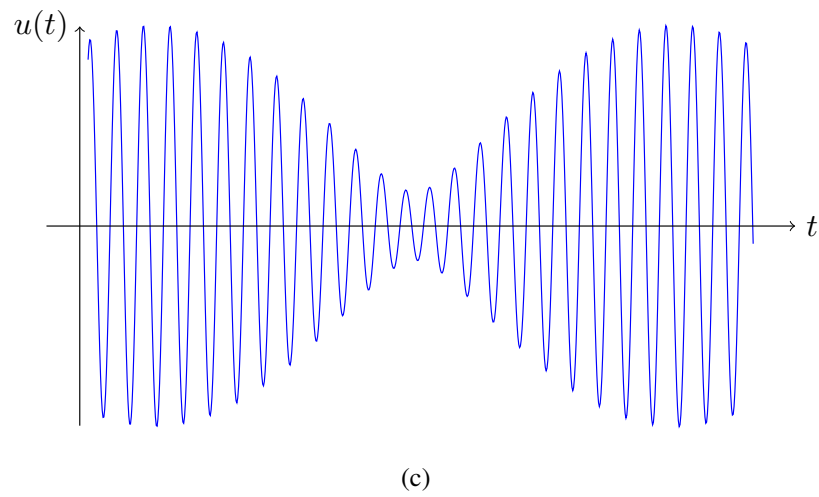
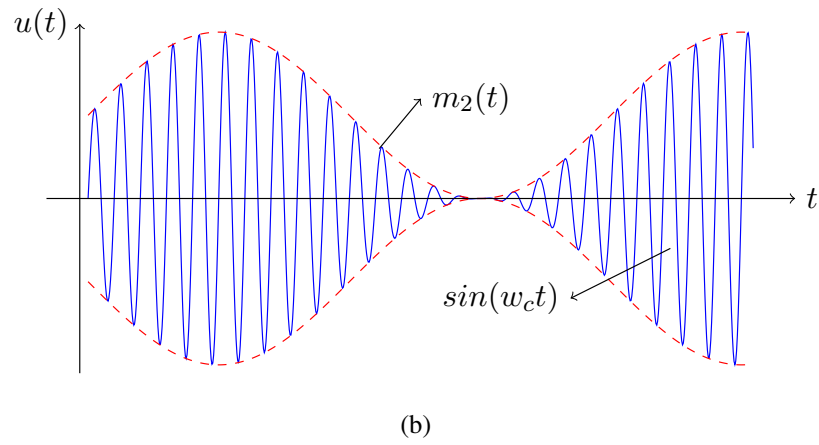
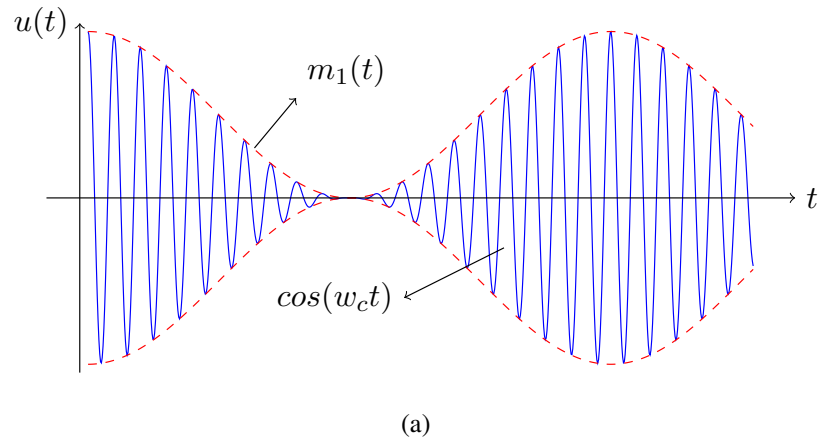


Figure 2.6 QAM signal construction (a) the carrier modulated  $m_1(t)$  signal (b) the quadrature carrier modulated  $m_2(t)$  signal and (c) QAM signal in the time domain

Suppose that the received signal is (2.16). To demodulate the message signal  $m_1(t)$ , the received signal is mixed with phase-coherent carrier signal  $\cos(\omega_c t)$ ,

$$\begin{aligned}\tilde{m}_1(t) &= u_{QAM}(t) \cos(\omega_c t) \\ &= [\cos(\omega_c t) + \sin(\omega_c t) + \cos((\omega_c - \omega_0)t)] \cos(\omega_c t) \\ &= \cos(\omega_c t) \cos(\omega_c t) + \sin(\omega_c t) \cos(\omega_c t) + \cos((\omega_c - \omega_0)t) \cos(\omega_c t)\end{aligned}\quad (2.17)$$

by using trigonometric identities, Equation (2.17) reduces to,

$$\tilde{m}_1(t) = \frac{1}{2} [1 + \cos(2\omega_c t) + \sin((\omega_c - \omega_c)t) + \sin(2\omega_c t) + \cos(\omega_0 t) + \cos((2\omega_c - \omega_0)t)] \quad (2.18)$$

by filtering out the high frequency and the DC components from (2.18), the message signal  $m_1(t)$ ,

$$m_1(t) = \frac{1}{2} \cos(\omega_0 t) \quad (2.19)$$

is obtained. To recover message signal  $m_2(t)$ , the received signal is mixed with the phase-coherent quadrature carrier signal  $\sin(\omega_c t)$ ,

$$\begin{aligned}\tilde{m}_1(t) &= u_{QAM}(t) \sin(\omega_c t) \\ &= [\cos(\omega_c t) + \sin(\omega_c t) + \cos((\omega_c - \omega_0)t)] \sin(\omega_c t) \\ &= \cos(\omega_c t) \sin(\omega_c t) + \sin(\omega_c t) \sin(\omega_c t) + \cos((\omega_c - \omega_0)t) \sin(\omega_c t)\end{aligned}\quad (2.20)$$

by using trigonometric identities, Equation (2.20) reduces to,

$$\tilde{m}_1(t) = \frac{1}{2} [1 - \cos(2\omega_c t) + \sin((\omega_c - \omega_c)t) + \sin(2\omega_c t) + \sin(\omega_0 t) + \sin((2\omega_c - \omega_0)t)]. \quad (2.21)$$

By filtering, the message signal  $m_2(t)$  is obtained.

$$m_2(t) = \frac{1}{2} \sin(\omega_0 t) \quad (2.22)$$



### CHAPTER THREE

#### DIRECTION OF ARRIVAL ESTIMATION

The signal processing of adaptive array antennas usually consists of parameter estimation and adaptive beamforming, both are based on the disposal of data induced by process of signal spatial sampling. The DoA estimation is a basic component of array signal processing and important in communication and radar systems including sonar, radio astronomy, seismology, navigation and surveillance systems. The received data at different antenna elements on array are phase-shifted according to signals DoA and the position of the antenna elements in space. There is one-to-one relationship between the direction of incoming signal and received data on each element. The relationship is inverted by array signal processing techniques to determine signal DoA. The DoA can be determined by spectral estimation methods that determine local maximums in spatial spectrum.

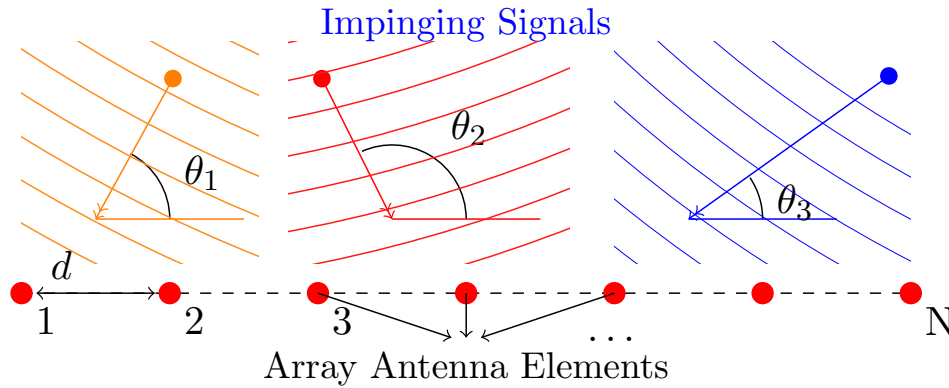


Figure 3.1 The DoA estimation problem

The problem set up is shown in Figure (3.1).  $M$  different signals are impinging on a linear, equispaced, antenna array with  $N$  elements, each with direction  $\theta_i$ . The goal of DoA estimation is to use the data received at the array to estimate direction of arrival angles  $\theta_i$ ,  $i = 1, \dots, M$ . The estimation is difficult because there are usually an unknown number of signals impinging on the array simultaneously, each from unknown directions with unknown amplitudes and the received signals are always corrupted by noise.

### 3.1 Model of Array Observation

The transmission of signals through wireless channel is very complex. The parametric model is obtained through simplifying the waveform transmission. The receiver characteristics of array element is only related to the location and is independent of physical size. In far-field conditions, the time delay of signal on each antenna element is determined by the array geometry and the direction of arrival of signal.

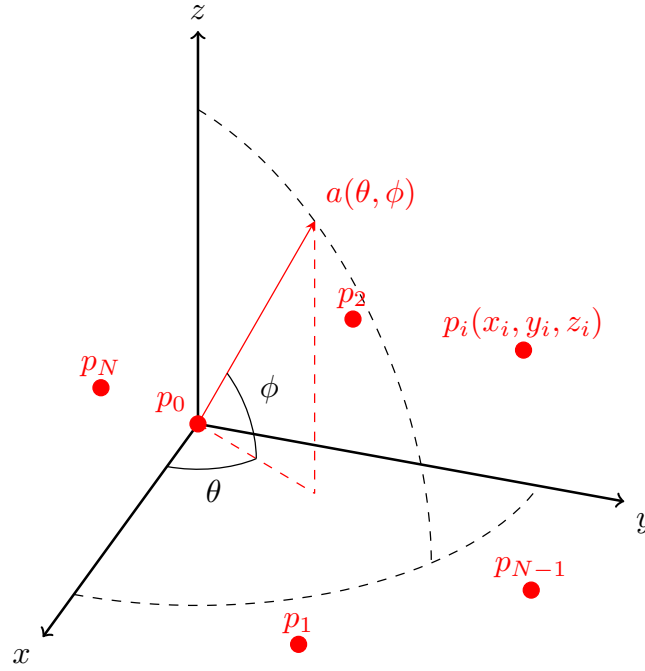


Figure 3.2 Array system geometry

The input is a plane wave propagating in direction  $\mathbf{a}(\phi, \theta)$  with angular frequency  $\omega$ .  $\mathbf{a}$  is a unit vector that can be expressed as:

$$\mathbf{a} = \begin{bmatrix} -\cos \phi \cos \theta \\ -\cos \phi \sin \theta \\ -\sin \phi \end{bmatrix} \quad (3.1)$$

Let the received signal by the origin sensor be  $x_0(t) = s(t)e^{j\omega t}$ . The array observation

vector can be written as:

$$\mathbf{x}(t) = x_0(t)e^{j\omega t} \begin{bmatrix} e^{-j\tau_1} \\ \vdots \\ e^{-j\tau_N} \end{bmatrix} \quad (3.2)$$

where  $\tau_i = \mathbf{a}^T \mathbf{p}_i / c$  is the time delay with respect to  $i^{th}$  sensor corresponding to the time of arrival at the origin sensor.  $c$  is the velocity of propagation in the medium and  $\mathbf{p}_i$  is sensors located at positions as shown in Figure (3.2),

$$\mathbf{p}_i = \begin{bmatrix} x_i \\ y_i \\ z_i \end{bmatrix} \quad (3.3)$$

The wave number  $\mathbf{k}$  is defined as  $\mathbf{k} = -2\pi\mathbf{a}/\lambda$ , therefore the  $N \times 1$  steering vector can be expressed as:

$$\mathbf{a}(\mathbf{k}) = \begin{bmatrix} e^{-j\mathbf{k}^T \mathbf{p}_1} \\ \vdots \\ e^{-j\mathbf{k}^T \mathbf{p}_N} \end{bmatrix} \quad (3.4)$$

Array signal processing is generally performed in the baseband. The vector (3.2) is expressed as  $\mathbf{x}(t) = \mathbf{x}_0(t)\mathbf{a}(\mathbf{k})$ . Thus, the  $N \times 1$  array observation is composed of complex expression of baseband signal and the steering vector. Hence, the steering vector is related to DoA and the array geometry.

### 3.1.1 Uniform Linear Array System

The Uniform Linear Array (ULA) is formed by antennas oriented along a line in space with uniform spacing. Let a ULA be composed of  $N$  antennas as shown in Figure (3.3), and let it receive  $M$  ( $M < N$ ) narrowband sources impinging from directions  $\phi_1, \dots, \phi_M$ . The  $N \times M$  matrix of steering vectors can be written as:

$$\mathbf{A}(\theta) = \begin{bmatrix} 1 & 1 & \dots & 1 \\ e^{-j\omega \frac{d \sin(\theta_1)}{c}} & e^{-j\omega \frac{d \sin(\theta_2)}{c}} & \dots & e^{-j\omega \frac{d \sin(\theta_M)}{c}} \\ \vdots & \vdots & \ddots & \vdots \\ e^{-j\omega(N-1) \frac{d \sin(\theta_1)}{c}} & e^{-j\omega(N-1) \frac{d \sin(\theta_2)}{c}} & \dots & e^{-j\omega(N-1) \frac{d \sin(\theta_M)}{c}} \end{bmatrix} \quad (3.5)$$

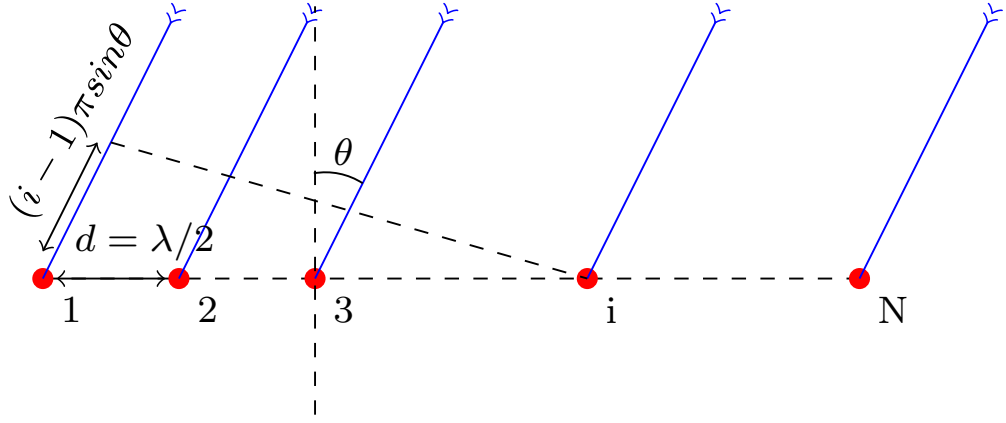


Figure 3.3 Uniform Linear Array antenna system

Assume that there are  $K$  snapshots  $s(1), s(2), \dots, s(K)$  available, so  $M \times K$  impinging signals matrix is

$$\mathbf{S} = \begin{bmatrix} s_1(1) & s_1(2) & \dots & s_1(K) \\ s_2(1) & s_2(2) & & s_2(K) \\ \vdots & \vdots & \ddots & \vdots \\ s_M(1) & s_M(2) & \dots & s_M(K) \end{bmatrix} \quad (3.6)$$

The  $N \times K$  array observation matrix is modeled as:

$$\mathbf{X}(t) = \mathbf{A}(\theta)\mathbf{S}(t) + \mathbf{N}(t) \quad (3.7)$$

where  $\mathbf{N}(t)$  represents the  $N \times K$  matrix of additive white Gaussian noise.

### 3.2 Amplitude Modulated Signal Received by ULA

Let impinging signal to the ULA be AM signal  $y(t)$  in Equation (2.4) with modulation index of 100% and  $\phi_c, \phi_m$  be equal zero. The received signal by  $i^{th}$  ( $i = 1, 2, \dots, N$ ) array element is defined as:

$$y(t - \tau_i) = [1 + \cos(\omega_m(t - \tau_i))]\cos(\omega_c(t - \tau_i)), \quad (3.8)$$

where  $\tau_i = (i - 1)d\sin(\theta)/c$ ,  $d$  is distance between array elements,  $c$  is the velocity of propagation in the medium.

The demodulation of received signal by  $i^{th}$  ULA element is:

$$\begin{aligned}
\tilde{y}(t) &= y(t - \tau_i) \cos(\omega_c t) \\
&= [1 + \cos(\omega_m(t - \tau_i))] \cos(\omega_c(t - \tau_i)) \cos(\omega_c t) \\
&= [1 + \cos(\omega_m(t - \tau_i))] \frac{1}{2} [\cos(-\omega_c \tau_i) + \cos(2\omega_c t - \omega_c \tau_i)] \\
&= \frac{1}{2} [\cos(\omega_c \tau_i) + \cos(2\omega_c t - \tau_i) + \cos(\omega_m t - \omega_m \tau_i) \cos(\omega_c \tau_i) + \\
&\quad \cos(\omega_m t - \omega_m \tau_i) \cos(2\omega_c t - \omega_c \tau_i)]
\end{aligned} \tag{3.9}$$

By filtering out the high frequency components and the DC component, the demodulated signal is:

$$\tilde{m}(t) = \frac{1}{2} \cos(\omega_m t - \omega_m \tau_i) \cos(\omega_c \tau_i), \tag{3.10}$$

The message signal is attenuated by the factor  $\cos(\omega_c \tau_i)$  and is time delayed by the factor  $\omega_m \tau_i$ . A PLL can be used to eliminate the attenuation factor and we have,

$$\tilde{m}(t) = \frac{1}{2} \cos(\omega_m t - \omega_m \tau_i), \tag{3.11}$$

The  $N \times M$  matrix of steering vectors is redefined according to AM modulated signal. The distance between the antenna elements in ULA is  $d = \lambda/2$  and where the signal wavelength is  $\lambda = c/f_c$ . The time delay and corresponding phase shift is

$$\omega_m \tau_i = \frac{2\pi f_m(i-1)\sin(\theta)}{2f_c} = \frac{(i-1)\pi f_m \sin(\theta)}{f_c} \tag{3.12}$$

where

$$\begin{aligned}
\tau_i &= (i-1)dsin(\theta)/c \\
&= (i-1)\sin(\theta)/(2f_c)
\end{aligned} \tag{3.13}$$

Hence, redefined  $N \times M$  matrix of steering vectors is

$$\mathbf{A}(\theta) = \begin{bmatrix} 1 & 1 & \dots & 1 \\ e^{-j\frac{\pi f_m \sin(\theta_1)}{f_c}} & e^{-j\frac{\pi f_m \sin(\theta_2)}{f_c}} & \dots & e^{-j\frac{\pi f_m \sin(\theta_M)}{f_c}} \\ \vdots & \vdots & \ddots & \vdots \\ e^{-j\frac{(N-1)\pi f_m \sin(\theta_1)}{f_c}} & e^{-j\frac{(N-1)\pi f_m \sin(\theta_2)}{f_c}} & \dots & e^{-j\frac{(N-1)\pi f_m \sin(\theta_M)}{f_c}} \end{bmatrix} \tag{3.14}$$

The redefined matrix of steering vectors is also valid for QAM modulated message signals. (3.14) is used during investigation of DoA angles by MUSIC algorithm.

### 3.3 Multiple Signal Classification

The MUSIC algorithm depends on the covariance matrix of the array observation matrix (3.7). The basic assumption of the MUSIC algorithm is that all noise vectors are orthogonal to the signal steering vectors. Using data model in (3.7) and assuming that the received signal waveform is a stationary process, the different signals are uncorrelated and noise vectors are zero mean, spatially white and statistically independent of source signals, the observation covariance matrix can be written as:

$$\begin{aligned}\mathbf{R} &= E[\mathbf{X}\mathbf{X}^H] \\ &= E[\mathbf{A}\mathbf{S}\mathbf{S}^H\mathbf{A}^H] + E[\mathbf{N}\mathbf{N}^H] \\ &= \mathbf{R}_s + \sigma_n^2\mathbf{I}\end{aligned}\tag{3.15}$$

where  $\mathbf{R}_s = E[\mathbf{A}\mathbf{S}\mathbf{S}^H\mathbf{A}^H]$   $N \times N$  signal covariance matrix with rank  $M$ ,  $\sigma_n^2$  noise variance,  $\mathbf{I}$  identity matrix,  $(\cdot)^H$  denotes Hermitian transpose and  $E[\cdot]$  is the expected value operator. Therefore it has  $N - M$  eigenvectors corresponding to the zero eigenvalues. Let  $\mathbf{q}_m$  be such an eigenvector. Therefore,

$$\begin{aligned}\mathbf{R}_s\mathbf{q}_m &= E[\mathbf{A}\mathbf{S}\mathbf{S}^H\mathbf{A}^H]\mathbf{q}_m = 0 \\ \Rightarrow E[\mathbf{q}_m^H\mathbf{A}\mathbf{S}\mathbf{S}^H\mathbf{A}^H\mathbf{q}_m] &= 0 \\ \Rightarrow \mathbf{A}^H\mathbf{q}_m &= 0\end{aligned}\tag{3.16}$$

where the final equation is valid since the matrix  $E[\mathbf{S}\mathbf{S}^H]$  is clearly positive definite. (3.16) implies that all  $N - M$  eigenvectors ( $\mathbf{q}_m$ ) of  $\mathbf{R}_s$  corresponding to the zero eigenvalues are orthogonal to all signal steering vectors. Let  $\mathbf{Q}_n$  be the  $N \times (N - M)$  matrix of these eigenvectors. The MUSIC maximizes the pseudo-spectrum,

$$P_{MUSIC}(\theta) = \frac{1}{\sum_{m=1}^{N-M} |\mathbf{A}^H(\theta)\mathbf{q}_m|^2} = \frac{1}{\mathbf{A}^H(\theta)\mathbf{Q}_n\mathbf{Q}_n^H\mathbf{A}(\theta)}\tag{3.17}$$

Note that since the eigenvectors composing  $\mathbf{Q}_n$  are orthogonal to the signal steering vectors, the denominator becomes zero when  $\theta$  is a signal direction. Therefore, the estimated signal directions are the  $M$  largest peaks in the pseudo-spectrum. However, in any practical situation, the signal covariance matrix  $\mathbf{R}_s$  is unavailable and must be estimated from the received signal  $\mathbf{X}$ . The key is that the eigenvectors of  $\mathbf{Q}_n$  can be

estimated using the eigenvectors of  $\mathbf{R}$ . For any eigenvector  $\mathbf{q}_m \in \mathbf{Q}$ ,

$$\begin{aligned}\mathbf{R}_s \mathbf{q}_m &= \lambda \mathbf{q}_m \\ \Rightarrow \mathbf{R} \mathbf{q}_m &= \mathbf{R}_s \mathbf{q}_m + \sigma^2 \mathbf{I} \mathbf{q}_m, \\ &= (\lambda + \sigma^2) \mathbf{q}_m\end{aligned}\tag{3.18}$$

any eigenvector of  $\mathbf{R}_s$  is also eigenvector of  $\mathbf{R}$  with corresponding eigenvalue  $\lambda + \sigma^2$ .

Let  $\mathbf{R}_s = \mathbf{Q} \mathbf{\Lambda} \mathbf{Q}^H$ . Therefore,

$$\begin{aligned}\mathbf{R} &= \mathbf{Q} [\mathbf{\Lambda} + \sigma^2 \mathbf{I}] \mathbf{Q}^H \\ &= \mathbf{Q} \begin{bmatrix} \lambda_1 + \sigma^2 & 0 & \dots & 0 & 0 & \dots & 0 \\ 0 & \lambda_2 + \sigma^2 & \dots & 0 & 0 & \dots & 0 \\ \vdots & \vdots & \ddots & \vdots & \vdots & \vdots & \vdots \\ 0 & 0 & \dots & \lambda_M + \sigma^2 & 0 & \dots & 0 \\ 0 & 0 & \dots & 0 & \sigma^2 & \dots & 0 \\ \vdots & \vdots & \vdots & \vdots & \vdots & \ddots & \vdots \\ 0 & 0 & \dots & 0 & 0 & \dots & \sigma^2 \end{bmatrix} \mathbf{Q}^H\end{aligned}\tag{3.19}$$

Based on this eigendecomposition, the eigenvector matrix  $\mathbf{Q}$  is separated into a signal matrix  $\mathbf{Q}_s$  with  $M$  columns, corresponding to the  $M$  signal eigenvalues, and a matrix  $\mathbf{Q}_n$ , with  $(N - M)$  columns, corresponding the noise eigenvalues ( $\sigma^2$ ). Note that  $\mathbf{Q}_n$ , the  $N \times (N - M)$  matrix of eigenvectors corresponding to the noise eigenvalue ( $\sigma^2$ ), is exactly the same as the matrix of eigenvectors  $\mathbf{R}_s$  corresponding to the zero-eigenvalue.  $\mathbf{Q}_s$  defines the signal subspace and  $\mathbf{Q}_n$  defines the noise subspace.

There are a number of important observations. The  $m^{th}$  signal eigenvalue is given by  $\lambda_m + \sigma^2$ . The smallest eigenvalues of  $\mathbf{R}$  are the noise eigenvalues and are all equal to  $\sigma^2$ . One way of distinguishing between the signal and noise eigenvalues (equivalently the signal and noise subspaces) is to determine the number of small eigenvalues that are equal. The orthogonality property of  $\mathbf{Q}$  yields that the signal subspace  $\mathbf{Q}_s$  and noise subspace  $\mathbf{Q}_n$  are perpendicular to each other.

Using the final two observations, it is seen that all noise eigenvectors are orthogonal to the signal steering vectors. MUSIC depend on this property of noise eigenvectors

and signal steering vectors. Consider the following function of  $\theta$ ,

$$\tilde{P}_{MUSIC}(\theta) = \frac{1}{\sum_{m=M+1}^N |\mathbf{q}_m^H \mathbf{A}(\theta)|^2} = \frac{1}{\mathbf{A}^H(\theta) \mathbf{Q}_n \mathbf{Q}_n^H \mathbf{A}(\theta)} \quad (3.20)$$

where  $\mathbf{q}_m$  is one of the noise eigenvectors. If  $\theta$  is equal to DoA of one of the signals,  $\mathbf{A}(\theta) \perp \mathbf{q}_m$  and the denominator is zero. Hence, the maxima of the function  $\tilde{P}_{MUSIC}(\theta)$  identifies the direction of arrival of signal.

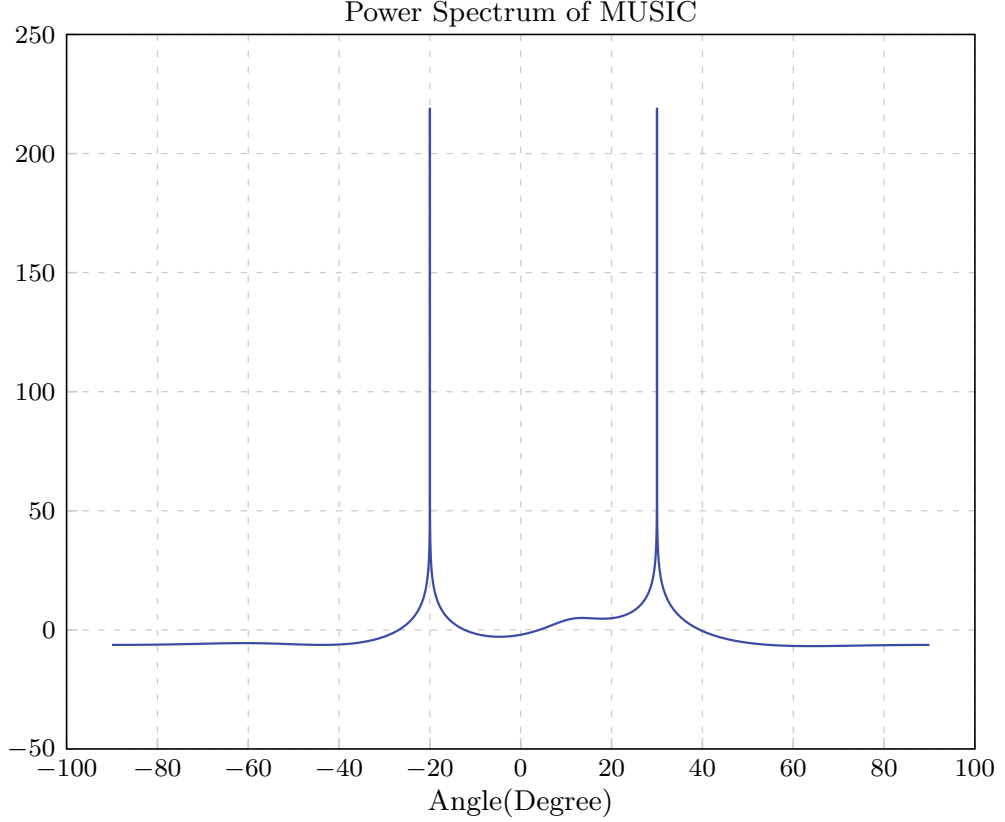


Figure 3.4 Spectrum of MUSIC function  $\tilde{P}_{MUSIC}(\theta)$ . The local maximas are the DoA of signals

The spectrum of the MUSIC function  $\tilde{P}_{MUSIC}(\theta)$  is shown in Figure (3.4). The MUSIC algorithm is executed over baseband signals. The SNR is 10 dB and signal frequencies are 1 MHz. The direction of arrival of impinging signals are  $-20^\circ$  and  $30^\circ$ , respectively.



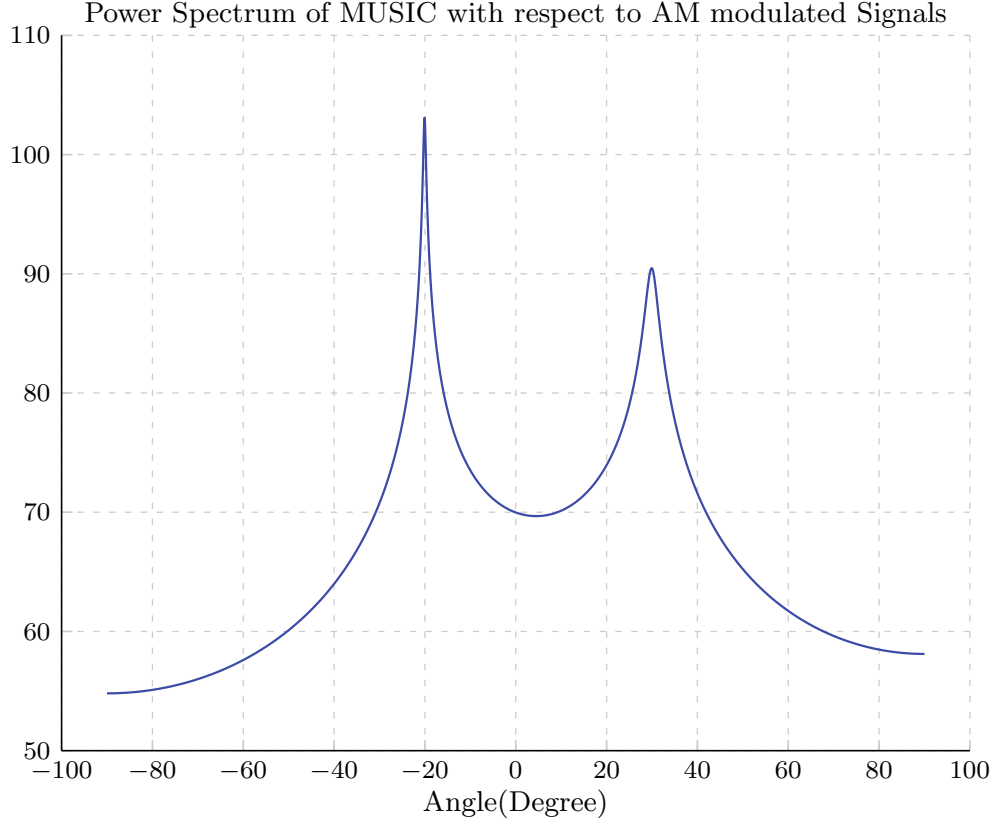


Figure 3.5 Spectrum of MUSIC function  $\tilde{P}_{MUSIC}(\theta)$  with respect to AM signals

The spectrum of the MUSIC function  $\tilde{P}_{MUSIC}(\theta)$  is shown in Figure (3.5). The MUSIC algorithm is executed over AM signals. The SNR is 50 dB and carrier frequency is 1 GHz. The message signal frequencies are 10 MHz and 10.1 MHz. The direction of arrival of impinging signals are  $-20^\circ$  and  $30^\circ$ , respectively.

## CHAPTER FOUR

### POSITION ESTIMATION

#### 4.1 Coordinate Systems and Transformations

##### 4.1.1 Coordinate Systems

A vector  $\mathbf{v} \in \mathbb{R}^3$  can be represented as a linear combination of three linearly independent basis vectors  $\mathbf{v}_1, \mathbf{v}_2, \mathbf{v}_3$ ,

$$\mathbf{v} = a_1 \mathbf{v}_1 + a_2 \mathbf{v}_2 + a_3 \mathbf{v}_3 \quad (4.1)$$

The scalars  $a_1, a_2, a_3$  are the coordinates of vector  $\mathbf{v}$ . Typically,  $\mathbf{v}_1 = [1, 0, 0]^T$ ,  $\mathbf{v}_2 = [0, 1, 0]^T$ ,  $\mathbf{v}_3 = [0, 0, 1]^T$  are chosen as linearly independent basis vectors.

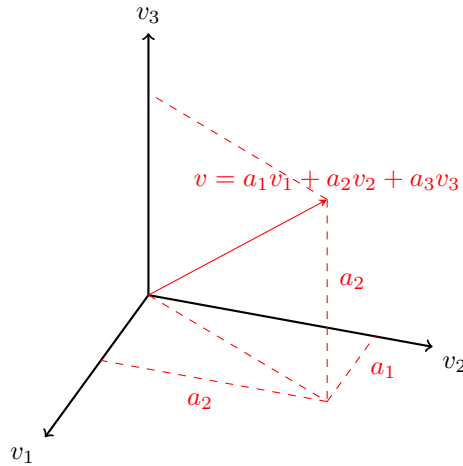


Figure 4.1 Coordinate system and basis vectors

Suppose the basis vectors  $\mathbf{v}_1, \mathbf{v}_2, \mathbf{v}_3$  are changed into new basis vectors  $\mathbf{u}_1, \mathbf{u}_2, \mathbf{u}_3$ . The new basis vectors can be expressed as combinations of the old basis vectors.

$$\mathbf{u}_1 = a_{11} \mathbf{v}_1 + a_{12} \mathbf{v}_2 + a_{13} \mathbf{v}_3 \quad (4.2)$$

$$\mathbf{u}_2 = a_{21} \mathbf{v}_1 + a_{22} \mathbf{v}_2 + a_{23} \mathbf{v}_3 \quad (4.3)$$

$$\mathbf{u}_3 = a_{31} \mathbf{v}_1 + a_{32} \mathbf{v}_2 + a_{33} \mathbf{v}_3 \quad (4.4)$$

and thus, the 3x3 change of basis matrix is obtained,

$$\mathbf{M} = \begin{bmatrix} a_{11} & a_{12} & a_{13} \\ a_{21} & a_{22} & a_{23} \\ a_{31} & a_{32} & a_{33} \end{bmatrix} \quad (4.5)$$

If the two representations of a given vector  $\mathbf{v}$  are

$$\mathbf{v} = \mathbf{a}^T \begin{bmatrix} v_1 \\ v_2 \\ v_3 \end{bmatrix}, \quad \text{and} \quad \mathbf{v} = \mathbf{b}^T \begin{bmatrix} u_1 \\ u_2 \\ u_3 \end{bmatrix}, \quad (4.6)$$

where  $\mathbf{a} = [a_1, a_2, a_3]^T$  and  $\mathbf{b} = [b_1, b_2, b_3]^T$ , then

$$\mathbf{v} = \mathbf{a}^T \begin{bmatrix} v_1 \\ v_2 \\ v_3 \end{bmatrix} = \mathbf{b}^T \begin{bmatrix} u_1 \\ u_2 \\ u_3 \end{bmatrix} = \mathbf{b}^T \mathbf{M} \begin{bmatrix} v_1 \\ v_2 \\ v_3 \end{bmatrix} \quad (4.7)$$

which implies that

$$\mathbf{a} = \mathbf{M}^T \mathbf{b} \quad \text{and} \quad \mathbf{b} = (\mathbf{M}^T)^{-1} \mathbf{a}. \quad (4.8)$$

Though the matrix  $\mathbf{M}$  could be used to rotate and scale vectors, it cannot deal with translation. In fact, an arbitrary affine transformation can be achieved via multiplication by a 3x3 matrix and shift by a vector.

#### 4.1.2 Affine Transformation

The transposed matrix simply represents an arbitrary affine transformation, having 12 degrees of freedom. These degrees of freedom can be viewed as the nine elements of a 3x3 matrix plus the three components of a vector shift.

$$\mathbf{M} = \begin{bmatrix} a_{11} & a_{21} & a_{31} & a_{41} \\ a_{12} & a_{22} & a_{32} & a_{42} \\ a_{13} & a_{23} & a_{33} & a_{43} \\ 0 & 0 & 0 & 1 \end{bmatrix} \quad (4.9)$$

The most important geometric transformations are rotations, scaling and translations and all affine transformations can be expressed as combinations of these

three. Affine transformations preserve line segments. If a line segment

$$P(a) = (1 - a)P_0 + aP_1 \quad (4.10)$$

is expressed in homogeneous coordinates as

$$\mathbf{p}(a) = (1 - a)\mathbf{p}_0 + a\mathbf{p}_1, \quad (4.11)$$

with respect to reference frame, then an affine transformation matrix  $\mathbf{M}$  sends the line segment  $P$  into the new line,

$$\mathbf{M}\mathbf{p}(a) = (1 - a)\mathbf{M}\mathbf{p}_0 + a\mathbf{M}\mathbf{p}_1 \quad (4.12)$$

Similarly, affine transformations map triangles to triangles and tetrahedra to tetrahedra.

#### 4.1.2.1 Translation

Translation is an operation that displaces points by a fixed distance in a given direction. If the displacement vector is  $\mathbf{d}$  then the point  $\mathbf{P}$  will be moved to

$$\mathbf{P}' = \mathbf{P} + \mathbf{d} \quad (4.13)$$

The (4.13) can be written in homogeneous coordinates as

$$\mathbf{p}' = \mathbf{p} + \mathbf{d}, \quad (4.14)$$

where

$$\mathbf{p} = \begin{bmatrix} x \\ y \\ z \\ 1 \end{bmatrix} \quad \mathbf{p}' = \begin{bmatrix} x' \\ y' \\ z' \\ 1 \end{bmatrix} \quad \mathbf{d} = \begin{bmatrix} a_x \\ a_y \\ a_z \\ 0 \end{bmatrix}$$

so that

$$x' = x + a_x \quad (4.15)$$

$$y' = y + a_y \quad (4.16)$$

$$z' = z + a_z \quad (4.17)$$

$$(4.18)$$

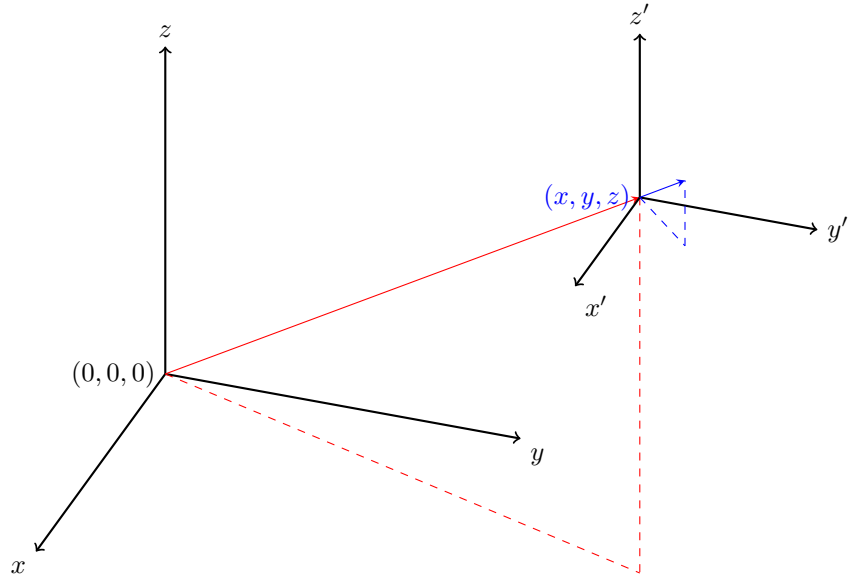


Figure 4.2 Translation of a point

Hence the transformation matrix  $\mathbf{T}$  which gives  $\mathbf{p}' = \mathbf{T}\mathbf{p}$  is clearly,

$$\mathbf{T}(a_x, a_y, a_z) = \begin{bmatrix} 1 & 0 & 0 & a_x \\ 0 & 1 & 0 & a_y \\ 0 & 0 & 1 & a_z \\ 0 & 0 & 0 & 1 \end{bmatrix} \quad (4.19)$$

which is called the translation matrix. The inverse of translation matrix is,

$$\mathbf{T}^{-1}(a_x, a_y, a_z) = \mathbf{T}(-a_x, -a_y, -a_z) \quad (4.20)$$

#### 4.1.2.2 Rotation

Rotation depends on an axis of rotation and the angle. Consider first rotation in the plane, about the origin. If a point  $(x, y) \in \mathbb{R}^2$  with coordinates

$$x = \rho \cos \phi \quad (4.21)$$

$$y = \rho \sin \phi \quad (4.22)$$

is rotated through an angle  $\theta$ , then the new position is  $(x', y')$ , where

$$x' = \rho \cos(\phi + \theta) \quad (4.23)$$

$$y' = \rho \sin(\phi + \theta) \quad (4.24)$$

Expanding these expressions,

$$x' = x \cos \theta - y \sin \theta \quad (4.25)$$

$$y' = x \sin \theta + y \cos \theta \quad (4.26)$$

or

$$\begin{bmatrix} x' \\ y' \end{bmatrix} = \begin{bmatrix} \cos \theta & -\sin \theta \\ \sin \theta & \cos \theta \end{bmatrix} \begin{bmatrix} x \\ y \end{bmatrix} \quad (4.27)$$

The rotation about  $x$  axis with rotation angle  $\alpha$  is shown in Figure (4.3) and the rotation matrix  $\mathbf{R}_x(\alpha)$  is given in (4.28)

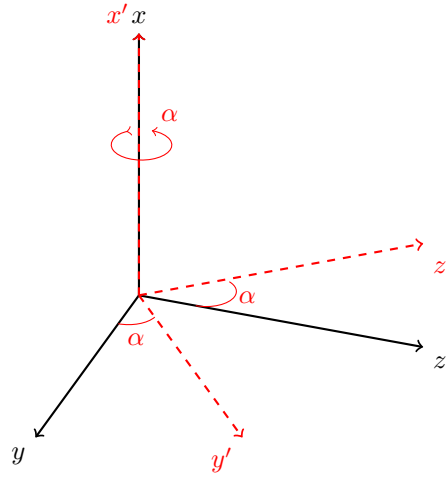


Figure 4.3 Rotation about the  $x$  axis

$$\mathbf{R}_x(\alpha) = \begin{bmatrix} 1 & 0 & 0 \\ 0 & \cos \alpha & -\sin \alpha \\ 0 & \sin \alpha & \cos \alpha \end{bmatrix} \quad (4.28)$$

The rotation about  $y$  axis with rotation angle  $\beta$  is shown in Figure (4.4) and the rotation matrix  $\mathbf{R}_y(\beta)$  is given in (4.29)

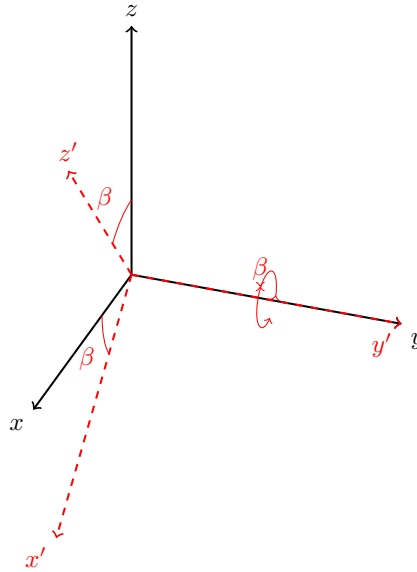


Figure 4.4 Rotation about the y axis

$$\mathbf{R}_y(\beta) = \begin{bmatrix} \cos\beta & 0 & \sin\beta \\ 0 & 1 & 0 \\ -\sin\beta & 0 & \cos\beta \end{bmatrix} \quad (4.29)$$

The rotation about  $z$  axis with rotation angle  $\gamma$  is shown in Figure (4.5) and the rotation matrix  $\mathbf{R}_z(\gamma)$  is given in (4.30)

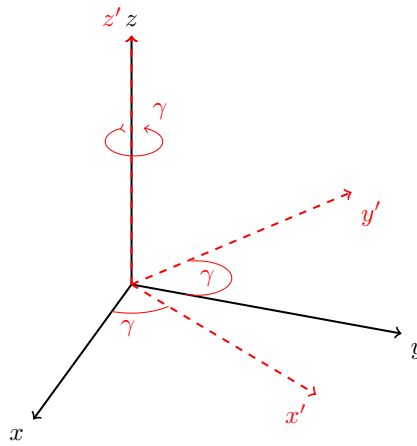


Figure 4.5 Rotation about the z axis

$$\mathbf{R}_z(\gamma) = \begin{bmatrix} \cos\gamma & -\sin\gamma & 0 \\ \sin\gamma & \cos\gamma & 0 \\ 0 & 0 & 1 \end{bmatrix} \quad (4.30)$$

Thus, the three rotation matrices corresponding to rotation about the  $x$ ,  $y$ ,  $z$  axes with rotation angles  $\alpha$ ,  $\beta$ ,  $\gamma$  in  $\mathbb{R}^3$  are  $\mathbf{R}_x(\alpha)$ ,  $\mathbf{R}_y(\beta)$ ,  $\mathbf{R}_z(\gamma)$ . The matrices result in positive rotations for positive  $\alpha$ ,  $\beta$ ,  $\gamma$  with respect to the right hand rule for the axes  $x$ ,  $y$ ,  $z$ .

#### 4.1.2.3 Combination of Rotation and Translation Matrix

A series of transformation on a point or object can be applied as a series of matrix multiplications. The combination of rotations and translation applied on a point is shown in Figure (4.6).

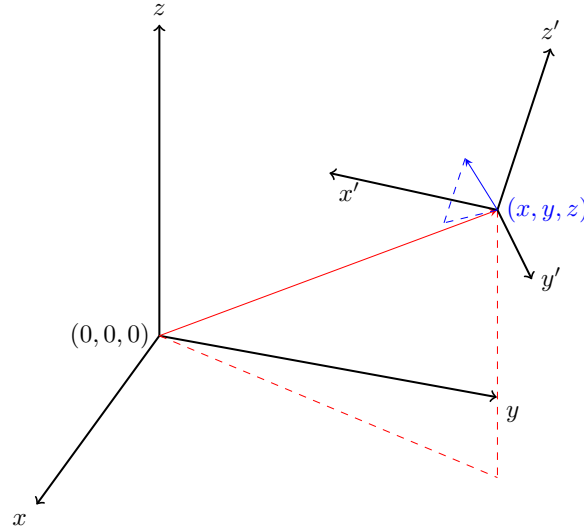


Figure 4.6 Affine transformation and combination of rotation and translation

To rotate an object about  $x$ ,  $y$ ,  $z$  axes with  $\alpha$ ,  $\beta$ ,  $\gamma$  angles, respectively, multiplication of matrices  $\mathbf{R}_x(\alpha)$ ,  $\mathbf{R}_y(\beta)$ ,  $\mathbf{R}_z(\gamma)$  gives

$$\mathbf{R}(\gamma, \beta, \alpha) = \mathbf{R}_z(\gamma) \mathbf{R}_y(\beta) \mathbf{R}_x(\alpha) \quad (4.31)$$

$$\mathbf{R}(\gamma, \beta, \alpha) = \begin{bmatrix} \cos \gamma & -\sin \gamma & 0 \\ \sin \gamma & \cos \gamma & 0 \\ 0 & 0 & 1 \end{bmatrix} \begin{bmatrix} \cos \beta & 0 & \sin \beta \\ 0 & 1 & 0 \\ -\sin \beta & 0 & \cos \beta \end{bmatrix} \begin{bmatrix} 1 & 0 & 0 \\ 0 & \cos \alpha & -\sin \alpha \\ 0 & \sin \alpha & \cos \alpha \end{bmatrix} \quad (4.32)$$



$$\mathbf{R}(\gamma, \beta, \alpha) = \begin{bmatrix} \cos \gamma \cos \beta & \cos \gamma \sin \beta \sin \alpha - \sin \gamma \cos \alpha & \cos \gamma \sin \beta \cos \alpha + \sin \gamma \sin \alpha \\ \sin \gamma \cos \beta & \sin \gamma \sin \beta \sin \alpha + \cos \gamma \cos \alpha & \sin \gamma \sin \beta \cos \alpha - \cos \gamma \sin \alpha \\ -\sin \beta & \cos \beta \sin \alpha & \cos \beta \cos \alpha \end{bmatrix} \quad (4.33)$$

Note that the order of the transformations is important, i.e. mathematically,

$$\mathbf{R}(\alpha, \beta, \gamma) \neq \mathbf{R}_x(\alpha) \mathbf{R}_y(\beta) \mathbf{R}_z(\gamma) \quad (4.34)$$

(4.33) can be represented as a geometric transformation matrix,

$$\mathbf{R}(\gamma, \beta, \alpha) = \begin{bmatrix} r_{11} & r_{12} & r_{13} & 0 \\ r_{21} & r_{22} & r_{23} & 0 \\ r_{31} & r_{32} & r_{33} & 0 \\ 0 & 0 & 0 & 1 \end{bmatrix} \quad (4.35)$$

the combination of rotation (4.35) and translation (4.19) matrices yields,

$$\begin{aligned} \mathcal{T}(\gamma, \beta, \alpha, x, y, z) &= \mathbf{R}_z(\gamma) \mathbf{R}_y(\beta) \mathbf{R}_x(\alpha) \mathbf{T}(x, y, z) \\ &= \mathbf{R}(\gamma, \beta, \alpha) \mathbf{T}(x, y, z) \end{aligned} \quad (4.36)$$

$$\mathcal{T}(\gamma, \beta, \alpha, x, y, z) = \begin{bmatrix} r_{11} & r_{12} & r_{13} & t_x \\ r_{21} & r_{22} & r_{23} & t_y \\ r_{31} & r_{32} & r_{33} & t_z \\ 0 & 0 & 0 & 1 \end{bmatrix} \quad (4.37)$$

## 4.2 Positioning

The rotation and translation properties of the geometric transformation matrix is used in positioning process. A point in global or referenced homogeneous coordinate system can be transformed to a new point in local homogeneous coordinate system or vice versa as shown in Figure (4.7).

Let  $P(x, y, z)$  be a point in global coordinate system whose basis vectors are  $x, y, z$  and  $P'(x', y', z')$  be a point in local coordinate system whose basis vectors are  $x', y', z'$  as shown in Figure (4.7). The point  $P'(x', y', z')$  is representation of the point  $P(x, y, z)$

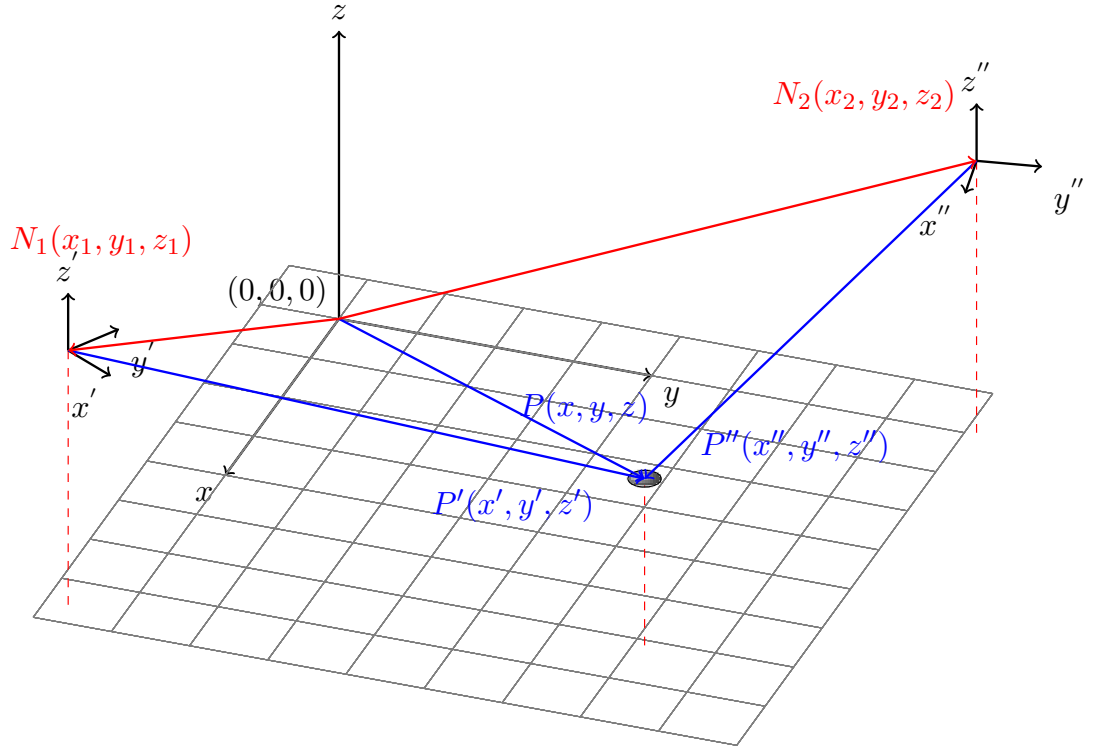


Figure 4.7 Representation of a point with respect to local and global coordinate systems in Cartesian coordinate notation

with respect to the local coordinates. The relation between these two points is defined by the geometric transform matrix,

$$\begin{aligned} \mathbf{P}'(x', y', z') &= \mathbf{R}(\gamma, \beta, \alpha) \mathbf{T}(x, y, z) \mathbf{P}(x, y, z) \\ &= \mathcal{T}(\gamma, \beta, \alpha, x, y, z) \mathbf{P}(x, y, z) \end{aligned} \quad (4.38)$$

$$\begin{bmatrix} x' \\ y' \\ z' \\ 1 \end{bmatrix} = \begin{bmatrix} r_{11} & r_{12} & r_{13} & t_x \\ r_{21} & r_{22} & r_{23} & t_y \\ r_{31} & r_{32} & r_{33} & t_z \\ 0 & 0 & 0 & 1 \end{bmatrix} \begin{bmatrix} x \\ y \\ z \\ 1 \end{bmatrix} \quad (4.39)$$

where  $\mathcal{T}(\gamma, \beta, \alpha, x, y, z)$  is geometric transformation matrix which includes necessary rotation and translation properties. The global to local transformation of points is invertible. Let  $\mathcal{T}_{10}(\gamma, \beta, \alpha, x, y, z)$  be transformation matrix which includes necessary rotation and translation parameters to transform points in local coordinates  $x', y', z'$

into global coordinates  $x, y, z$ ,

$$\mathcal{T}_{10}(\gamma, \beta, \alpha, x, y, z) = \begin{bmatrix} r'_{11} & r'_{12} & r'_{13} & t'_x \\ r'_{21} & r'_{22} & r'_{23} & t'_y \\ r'_{31} & r'_{32} & r'_{33} & t'_z \\ 0 & 0 & 0 & 1 \end{bmatrix} \quad (4.40)$$

Let  $\mathcal{T}_{20}(\gamma, \beta, \alpha, x, y, z)$  be transformation matrix which includes necessary rotation and translation parameters to transform points in local coordinates  $x'', y'', z''$  into global coordinates  $x, y, z$ ,

$$\mathcal{T}_{20}(\gamma, \beta, \alpha, x, y, z) = \begin{bmatrix} r''_{11} & r''_{12} & r''_{13} & t''_x \\ r''_{21} & r''_{22} & r''_{23} & t''_y \\ r''_{31} & r''_{32} & r''_{33} & t''_z \\ 0 & 0 & 0 & 1 \end{bmatrix} \quad (4.41)$$

Using the transformation matrices (4.40) and (4.41), the point  $P(x, y, z)$  in global coordinates can be expressed as

$$P(x, y, z) = \mathcal{T}_{10} P'(x', y', z') = \mathcal{T}_{20} P''(x'', y'', z'') \quad (4.42)$$

$$\begin{bmatrix} x \\ y \\ z \\ 1 \end{bmatrix} = \mathcal{T}_{10} \begin{bmatrix} x' \\ y' \\ z' \\ 1 \end{bmatrix} = \mathcal{T}_{20} \begin{bmatrix} x'' \\ y'' \\ z'' \\ 1 \end{bmatrix} \quad (4.43)$$

#### 4.2.1 Positioning via Direction of Arrival

The designed antenna system and the DoA algorithm provide the azimuth and the elevation angles in the local nodes and the reference node with respect to their local coordinate systems. Therefore, the spherical coordinate system  $\theta, \phi, R$  is suitable to define the points in nodes where,  $\theta$  azimuth angle is the angle from positive  $x$ -axis towards the positive  $y$ -axis,  $\phi$  elevation angle is the angle from  $xy$  plane towards the positive  $z$ -axis and  $R$  is distance from the origin as shown in Figure (4.8).

The problem set up is shown in Figure (4.8). To locate the point in 3-D space, the azimuth, the elevation and the distance from the origin must be known. The designed

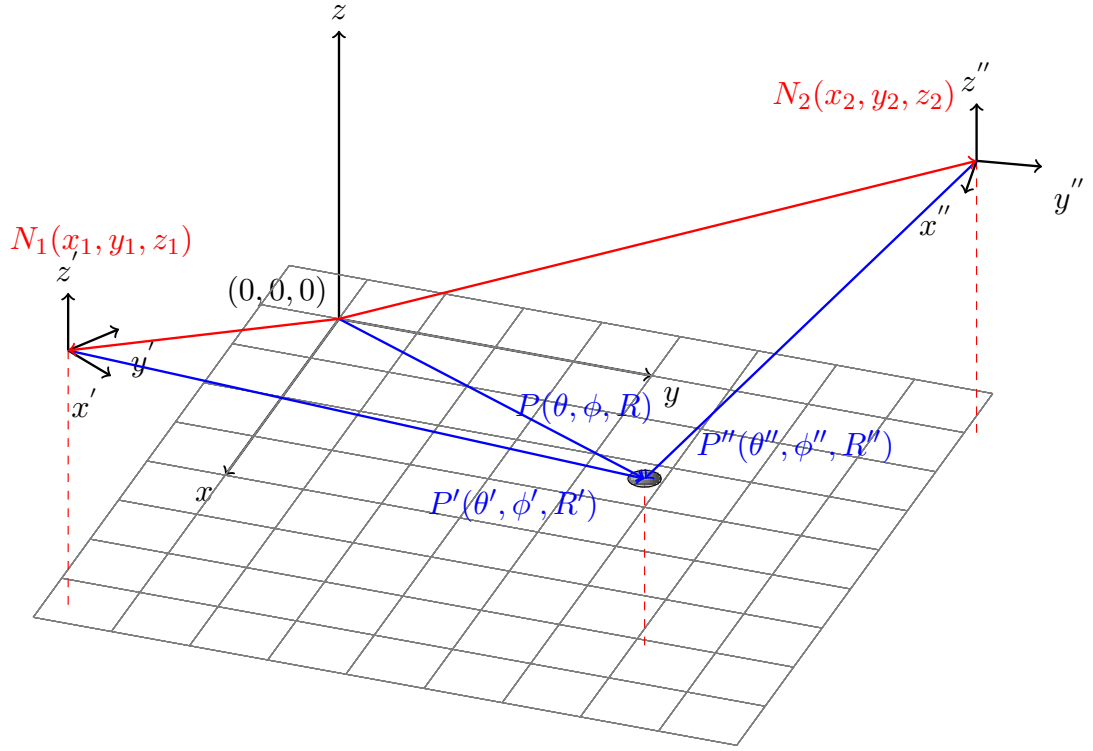


Figure 4.8 The positioning of a point represented in spherical coordinate notation with respect to local and global coordinate system

system provides the azimuth  $\theta$  and the elevation  $\phi$  angles. The distance from origin  $R$  must be determined in 3-D space. Let a point  $P(\theta, \phi, R)$  be represented with respect to the coordinate system  $x, y, z$  and its representation in the coordinate systems  $x', y', z'$  and  $x'', y'', z''$  are  $P'(\theta', \phi', R')$  and  $P''(\theta'', \phi'', R'')$ , respectively. Using transform matrices in (4.40) and (4.41),

$$P(\theta, \phi, R) = \mathcal{T}_{10} P'(\theta', \phi', R') = \mathcal{T}_{20} P''(\theta'', \phi'', R'') \quad (4.44)$$

where

$$P(\theta, \phi, R) = \begin{bmatrix} R \cos \phi \cos \theta \\ R \cos \phi \sin \theta \\ R \sin \phi \\ 1 \end{bmatrix}, \quad P'(\theta', \phi', R') = \begin{bmatrix} R' \cos \phi' \cos \theta' \\ R' \cos \phi' \sin \theta' \\ R' \sin \phi' \\ 1 \end{bmatrix},$$

and

$$P''(\theta'', \phi'', R'') = \begin{bmatrix} R'' \cos \phi'' \cos \theta'' \\ R'' \cos \phi'' \sin \theta'' \\ R'' \sin \phi'' \\ 1 \end{bmatrix}$$

Moreover, the point  $P(\theta, \phi, R)$  can be expressed, as

$$P(\theta, \phi, R) = \frac{1}{2} [\mathcal{T}_{10} P(\theta', \phi', R') + \mathcal{T}_{20} P(\theta'', \phi'', R'')]. \quad (4.45)$$

By expanding (4.45), we get

$$\begin{aligned} 2R \cos \phi \cos \theta &= R' r'_{11} \cos \phi' \cos \theta' + R' r'_{12} \cos \phi' \sin \theta' + R' r'_{13} \sin \phi' + t'_x \\ &+ R'' r''_{11} \cos \phi'' \cos \theta'' + R'' r''_{12} \cos \phi'' \sin \theta'' + R'' r''_{13} \sin \phi'' + t''_x \end{aligned} \quad (4.46)$$

$$\begin{aligned} 2R \cos \phi \sin \theta &= R' r'_{21} \cos \phi' \cos \theta' + R' r'_{22} \cos \phi' \sin \theta' + R' r'_{23} \sin \phi' + t'_y \\ &+ R'' r''_{21} \cos \phi'' \cos \theta'' + R'' r''_{22} \cos \phi'' \sin \theta'' + R'' r''_{23} \sin \phi'' + t''_y \end{aligned} \quad (4.47)$$

$$\begin{aligned} 2R \sin \phi &= R' r'_{31} \cos \phi' \cos \theta' + R' r'_{32} \cos \phi' \sin \theta' + R' r'_{33} \sin \phi' + t'_z \\ &+ R'' r''_{31} \cos \phi'' \cos \theta'' + R'' r''_{32} \cos \phi'' \sin \theta'' + R'' r''_{33} \sin \phi'' + t''_z \end{aligned} \quad (4.48)$$

and by algebraic manipulations of (4.46), (4.47) and (4.48) we obtain

$$\begin{aligned} -t'_x - t''_x &= -2R \cos \phi \cos \theta + R'(r'_{11} \cos \phi' \cos \theta' + r'_{12} \cos \phi' \sin \theta' + r'_{13} \sin \phi') \\ &+ R''(r''_{11} \cos \phi'' \cos \theta'' + r''_{12} \cos \phi'' \sin \theta'' + r''_{13} \sin \phi'') \end{aligned} \quad (4.49)$$

$$\begin{aligned} -t'_y - t''_y &= -2R \cos \phi \sin \theta + R'(r'_{21} \cos \phi' \cos \theta' + r'_{22} \cos \phi' \sin \theta' + r'_{23} \sin \phi') \\ &+ R''(r''_{21} \cos \phi'' \cos \theta'' + r''_{22} \cos \phi'' \sin \theta'' + r''_{23} \sin \phi'') \end{aligned} \quad (4.50)$$

$$\begin{aligned} -t'_z - t''_z &= -2R \sin \phi + R'(r'_{31} \cos \phi' \cos \theta' + r'_{32} \cos \phi' \sin \theta' + r'_{33} \sin \phi') \\ &+ R''(r''_{31} \cos \phi'' \cos \theta'' + r''_{32} \cos \phi'' \sin \theta'' + r''_{33} \sin \phi'') \end{aligned} \quad (4.51)$$

(4.49), (4.50) and (4.51) can be expressed as a system of linear equations,

$$\begin{bmatrix} -2 \cos \phi \cos \theta & r'_{11} \cos \phi' \cos \theta' + r'_{12} \cos \phi' \sin \theta' + r'_{13} \sin \phi' \\ -2 \cos \phi \sin \theta & r'_{21} \cos \phi' \cos \theta' + r'_{22} \cos \phi' \sin \theta' + r'_{23} \sin \phi' \\ -2 \sin \phi & r'_{31} \cos \phi' \cos \theta' + r'_{32} \cos \phi' \sin \theta' + r'_{33} \sin \phi' \end{bmatrix} \begin{bmatrix} R \\ R' \\ R'' \end{bmatrix} = \begin{bmatrix} -t'_x - t''_x \\ -t'_y - t''_y \\ -t'_z - t''_z \end{bmatrix} \quad (4.52)$$

By reducing (4.52), the system of linear equations is obtained as

$$\mathbf{A}(\theta, \phi, \alpha, \beta, \gamma) \mathbf{r} = \mathbf{t}(x, y, z) \quad (4.53)$$

where  $\mathbf{t}(x, y, z)$  is sum of translation vector of the local nodes with respect to reference system,  $\mathbf{A}(\theta, \phi, \alpha, \beta, \gamma)$  is calculated with respect to rotation matrix and the azimuth and elevation angles are obtained by estimation of direction of arrival and  $\mathbf{r}$  is unknown vector of distances with respect to local origins and the reference. Simply,  $\mathbf{r}$  is obtained by solving the system of linear equations (4.53). The position of the point  $P(\theta, \phi, R)$  is calculated via estimation of the direction of arrival angles.

## CHAPTER FIVE

### HARDWARE DESIGN

The hardware of the radio source positioning system has been designed according to the requirements of the radio source positioning system. The radio source positioning system includes two parts; a RF radio source and at least two receiver nodes. Hence, the hardware design consists of two parts, the design of RF radio source and the design of receiver node. The designs of the RF radio source and the receiver unit have been shown in Figure (5.1a) and Figure (5.1b), respectively. The receiver nodes consist of five receiver units which corresponds to the number of the inset-fed microstrip patch antennas in an antenna array system.

The RF radio source has three parts; a intermediate frequency (IF) block, a RF front-end and a inset-fed microstrip patch antenna. The IF block consists of a baseband signal source and a  $3^{rd}$  order Chebyshev lowpass filter. The RF front-end consists of an IQ modulator (quadrature modulator), a RF driver amplifier, a  $3^{rd}$  order Chebyshev bandpass filter. The RF front-end and the inset-fed patch antenna have been designed to work at 2.41 GHz. Because, the radio band between 2.4 GHz and 2.5 GHz is reserved for industrial, scientific and medical use. This radio band is also called as industrial, scientific and medical (ISM) radio band.

An ADRF6703 quadrature modulator integrated circuit (IC) has been used at the design of the RF front-end to modulate the baseband signal to the RF frequency. The ADRF6703 IC is a 1.55 GHz to 2.65 GHz quadrature modulator with 2.1 GHz to 2.6 GHz fractional-N PLL and integrated voltage controlled oscillator (VCO). The design of the RF driver amplifier has been made using an ADL5320 IC which is a 0.4 GHz to 2.7 GHz RF driver amplifier.

The IF block of the receiver unit consists of a processing unit, an analog to digital converter (ADC) and a  $3^{rd}$  order Chebyshev lowpass filter. The processing unit includes a microcontroller unit such as Beaglebone black for data acquisition and signal processing. An AD9238 ADC IC has been used in the design to convert analog IF signal to digital.

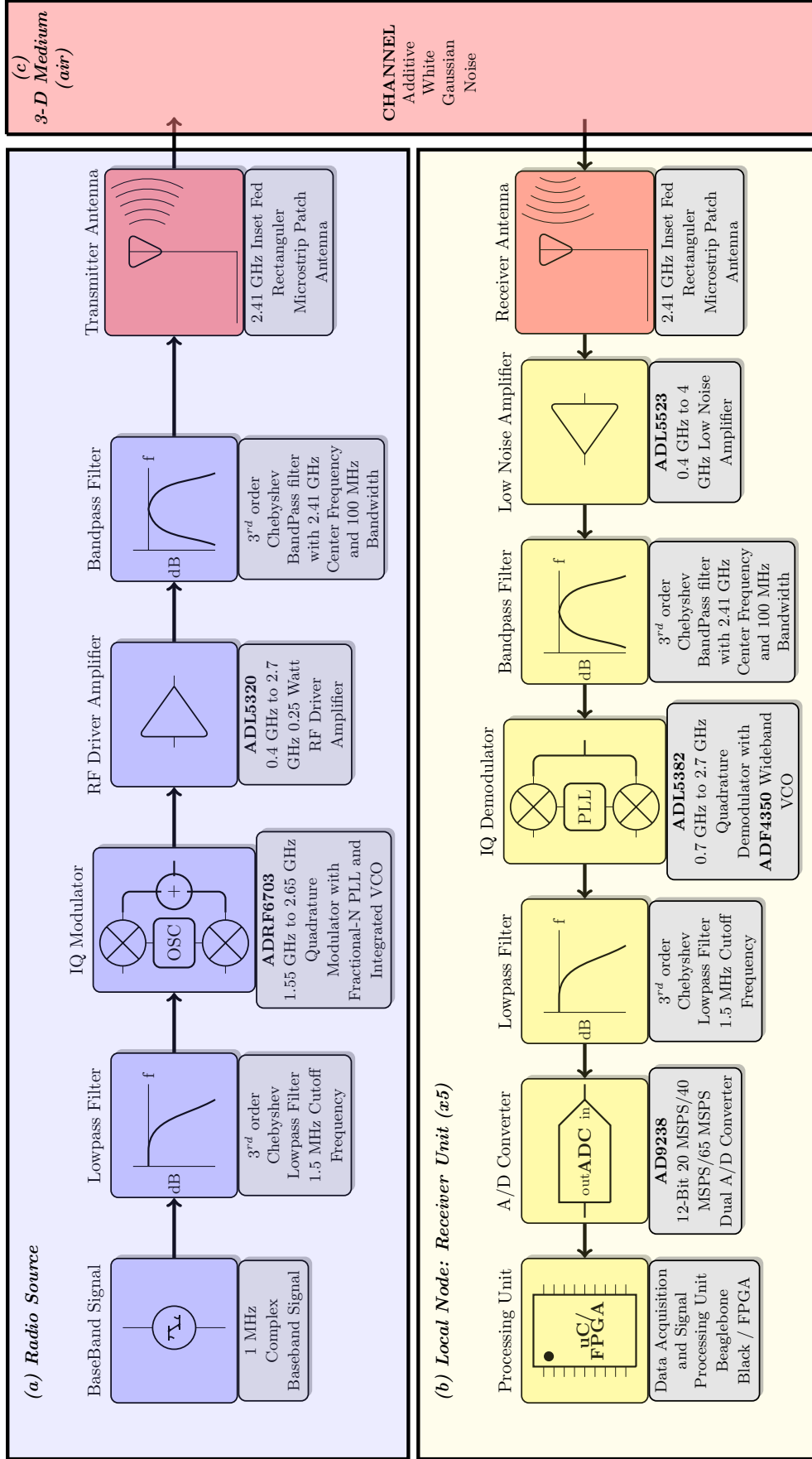


Figure 5.1 The hardware design of the radio source positioning system (a) the RF radio source (b) the receiver unit (c) AWGN channel



The RF front-end of the receiver unit consists of an IQ demodulator (quadrature demodulator), a 3<sup>rd</sup> order Chebyshev bandpass filter, a low noise amplifier. An ADL5382 quadrature demodulator IC has been used in the design of the RF front-end with an ADF4350 wideband VCO IC to demodulate the QAM signal received by the inset-fed patch antenna. The design of the low noise amplifier has been made using ADL5523 IC which is a 0.4 GHz to 4 GHz low noise amplifier (LNA).

The RF front-end of the radio source and the receiver units have been designed using the ANSYS DESIGNER software. Also, the performance assessments of the designs have been made using the ANSYS DESIGNER software. The design of inset-fed microstrip patch antenna and performance assessment of the patch antennas have been made using the ANSYS HFSS software.

### 5.1 Inset Fed Microstrip Patch Antenna Design

Microstrip patch antennas are used for various wireless applications due to high transmission frequency, low fabrication cost, light weight, planar structure and ease of integration with microwave circuits (Balanis, 1997). A microstrip patch antenna consists of a radiating patch on one side of dielectric substrate which has a grounded plane on other side as shown in Figure (5.2). The inset fed provides impedance control over microstrip patch to match impedance of the patch antenna to the excitation system.

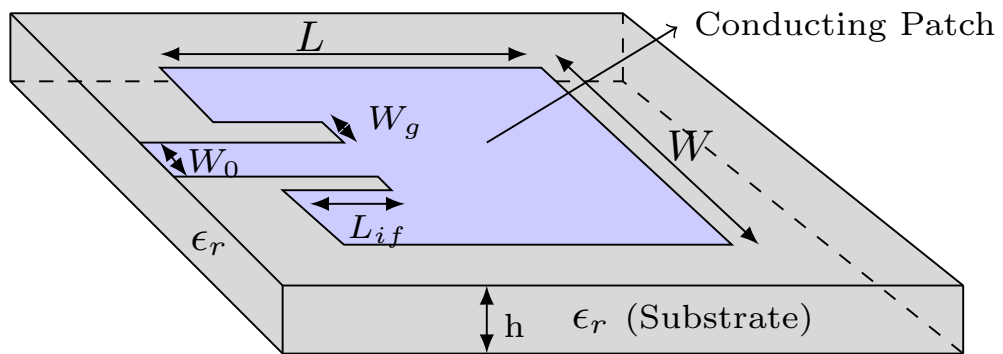


Figure 5.2 The inset-fed microstrip patch antenna geometry

The characteristics of microstrip patch antenna are basically defined by its geometry and material properties of the substrate. The basic antenna parameters are the patch length  $L$  and the width  $W$ , the dielectric constant of the substrate  $\epsilon_r$  and the height of dielectric substrate  $h$  as shown in Figure (5.2). The design procedure starts with calculating  $W$

$$W = \frac{1}{2f_r \sqrt{\mu_0 \epsilon_0}} \sqrt{\frac{2}{\epsilon_r + 1}} = \frac{c_0}{2f_r} \sqrt{\frac{2}{\epsilon_r + 1}} \quad (5.1)$$

where  $c_0 = 1/\sqrt{\mu_0 \epsilon_0}$  is the speed of light in free-space and  $f_r$  is the resonant frequency of the patch antenna. The effective dielectric constant of the patch antenna  $\epsilon_{eff}$  is determined approximately by

$$\epsilon_{eff} = \frac{\epsilon_r + 1}{2} + \frac{\epsilon_r - 1}{2} \left[ 1 + 12 \frac{h}{W} \right]^{-1/2} \quad (5.2)$$

The length of the patch antenna  $L$  is calculated by

$$L = \frac{c_0}{2f_r \sqrt{\epsilon_{eff}}} - 2\Delta L \quad (5.3)$$

where  $\Delta L$  is extension of length,

$$\Delta L = 0.412h \frac{(\epsilon_{eff} + 0.3) \left( \frac{W}{h} + 0.264 \right)}{(\epsilon_{eff} - 0.258) \left( \frac{W}{h} + 0.8 \right)} \quad (5.4)$$

To provide maximum power transfer, the resonant input impedance of the designed patch antenna must be matched to characteristic impedance of the excitation system.

The resonant input resistance is determined by

$$R_{in} = \frac{1}{2(G_1 + G_{12})} \quad (5.5)$$

where,  $G_1$  is conductance which is calculated by

$$G_1 = \frac{W}{120\lambda_0} \left[ 1 - \frac{1}{24}(k_0 h)^2 \right] \quad \frac{h}{\lambda_0} < \frac{1}{10} \quad (5.6)$$

and  $G_{12}$  is mutual conductance which is calculated by

$$G_{12} = \frac{1}{120\pi^2} \int_0^\pi \left[ \frac{\sin\left(\frac{k_0 W}{2} \cos \theta\right)}{\cos \theta} \right]^2 J_0(k_0 L \sin \theta) \sin^3 \theta d\theta. \quad (5.7)$$

$J_0$  is the Bessel function of the first kind of order zero,  $\lambda_0$  is the free-space wavelength of signal and  $k_0 = 2\pi/\lambda_0$  is the phase constant. The resonant input resistance can be

changed by using an inset feed whose length is  $L_{if}$ . This is used to match the patch antenna using a microstrip line feed whose characteristic impedance  $Z_0$  is given as

$$Z_0 = \begin{cases} \frac{60}{\sqrt{\epsilon_{eff}}} \ln \left[ \frac{8h}{W_0} + \frac{W_0}{4h} \right] & \frac{W_0}{h} \leq 1 \\ \frac{120\pi}{\sqrt{\epsilon_{eff}} \left[ \frac{W_0}{h} + 1.393 + 0.667 \ln \left( \frac{W_0}{h} + 1.444 \right) \right]} & \frac{W_0}{h} > 1 \end{cases} \quad (5.8)$$

where  $W_0$  is the width of the microstrip line, as shown in Figure (5.2). The input resistance for the inset feed is given by

$$R_{in}(L_{if}) = \frac{1}{2(G_1 + G_{12})} \cos^2 \left( \frac{\pi}{L} L_{if} \right) \quad (5.9)$$

or the length of the inset feed is determined by

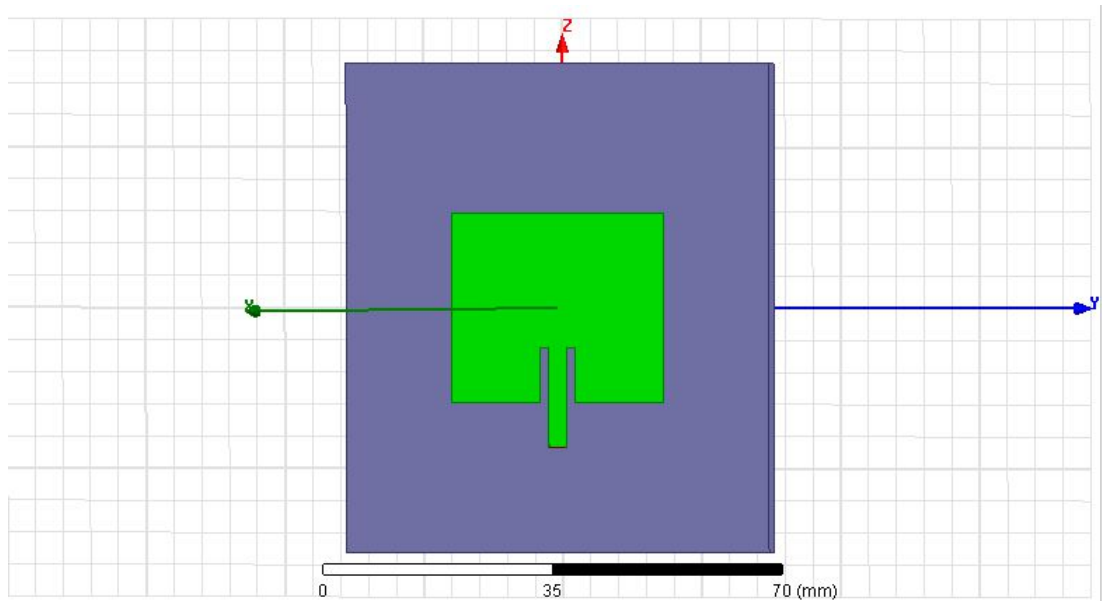
$$L_{if} = \frac{L}{\pi} \arccos \left( \sqrt{\frac{Z_0}{R_{in}}} \right) \quad (5.10)$$

where  $Z_0$  characteristic impedance of microstrip line,  $R_{in}$  resonant input impedance and  $L$  length of the patch antenna (Balanis, 1997; Pozar, 2005).

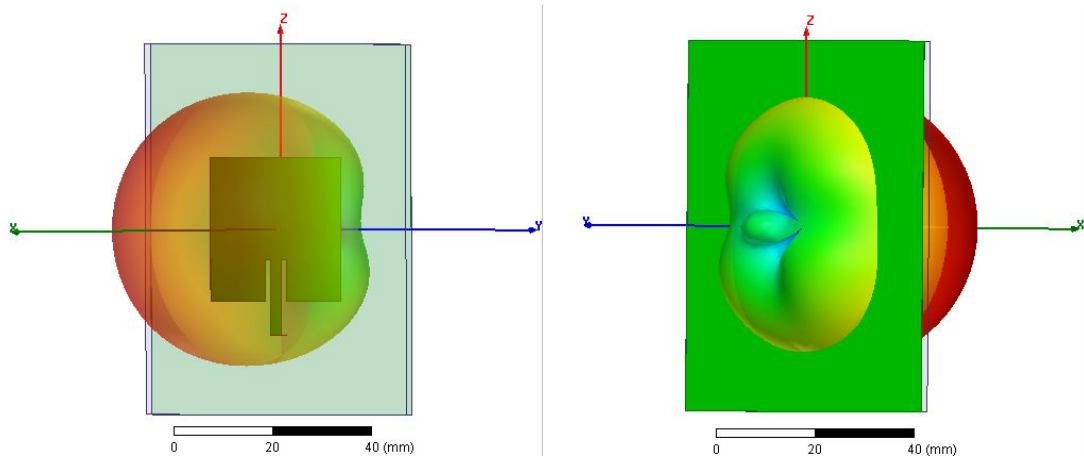
### 5.1.1 2.41 GHz Inset Fed Microstrip Patch Antenna Design

A inset-fed microstrip patch antenna has been designed to meet the requirements of the radio source positioning system. The antenna array system is formed by the inset-fed microstrip patch antennas. The patch antenna has been designed using a substrate (FR4) whose dielectric constant  $\epsilon_r$  is 4.3 and height of substrate is 1.57 mm by following the procedure which is described in Section (5.1). The resonant frequency  $f_r$  is 2.41 GHz and the characteristic impedance of the microstrip line  $Z_0$  is 50 Ohm.

A Matlab script has been written to calculate the basic patch antenna parameters and inset-fed length according to the design specifications. The calculated parameters are given in Table (5.1). The 3D model of the inset-fed microstrip patch antenna has been created using ANSYS HFSS software with respect to calculated parameters as shown in Figure (5.3a). The software has also been used to simulate and examine the performance of the patch antenna.



(a)



(b)

(c)

Figure 5.3 (a) The inset-fed microstrip patch antenna Ansoft Hfss model (b) The radiation pattern of the designed patch antenna (front) (c) The radiation pattern of patch antenna (back)

Table 5.1 The basic parameters of patch antenna which are calculated using Matlab script

Inset-fed microstrip patch antenna parameters					
$W$ (mm)	$L$ (mm)	$R_{in}$ (Ohm)	$L_{if}$ (mm)	$W_0$ (mm)	$W_g$ (mm)
38.10	29.54	195.95	9.79	3.06	1.53

Frequency domain simulations have been performed using the ANSYS HFSS to investigate the resonance frequency of the patch antenna and the matching between the antenna and the 50 *Ohm* microstrip feed line. The simulation results have not met the design specifications. It has been observed that the resonant frequency slightly deviates from the desired frequency. Also, the match between the patch antenna and the microstrip feed line has not been possible, initially.

A parametric 3D model of the patch antenna has been created and a combination of frequency sweep and parameter sweep simulations has been performed to optimize the geometry of the antenna with respect to the design specifications. The length of the inset-fed has been chosen as a parameter for the parameter sweep simulation to search optimum  $L_{if}$  which provides matching between the antenna and the microstrip feed line. The interval of  $L_{if}$  has been chosen as 2 *mm* to 12 *mm* with 0.1 *mm* steps. The frequency sweep simulation has been performed to search resonant frequency of antenna when the antenna and the feed line has been matched. The interval of frequency sweep has been chosen as 2.38 *GHz* and 2.44 *GHz* with 1 *MHz* steps.

The frequency sweep simulations have been performed for each value of  $L_{if}$ . The minimum values of voltage standing wave ratio (VSWR) of the patch antenna has been determined for each frequency sweep simulation by searching the frequency response of the patch antenna. The minimum values of VSWR have been plotted with respect to the value of  $L_{if}$  as shown in Figure (5.4). Likewise, the minimum values of  $S_{11}$  scattering parameter (S-parameter) of the patch antenna have been plotted with respect to the value of  $L_{if}$  as shown in Figure (5.5).

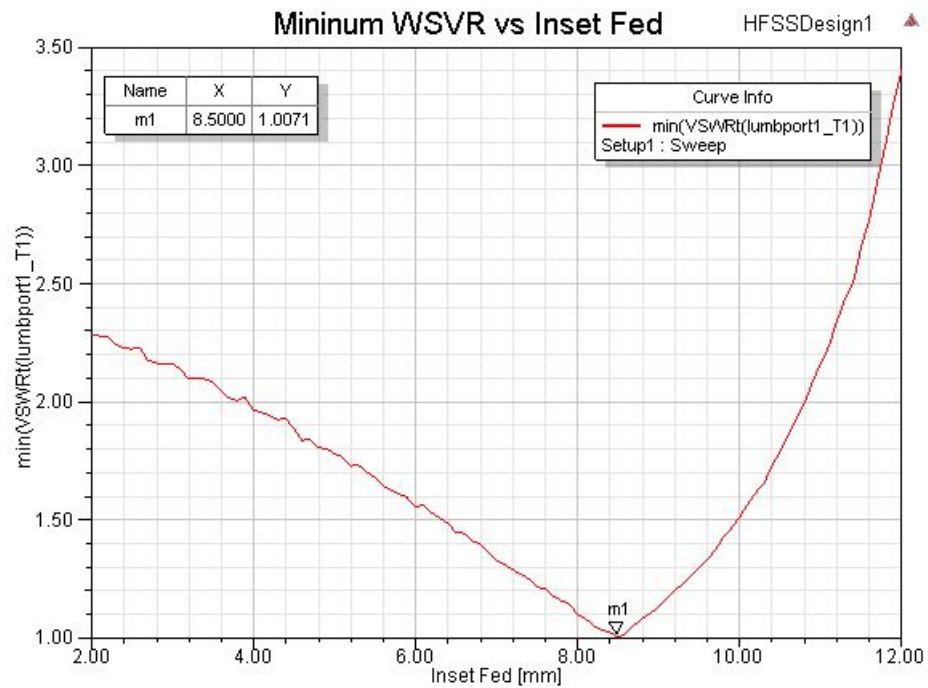


Figure 5.4 The minimum VSWR of the patch antenna versus inset-fed length

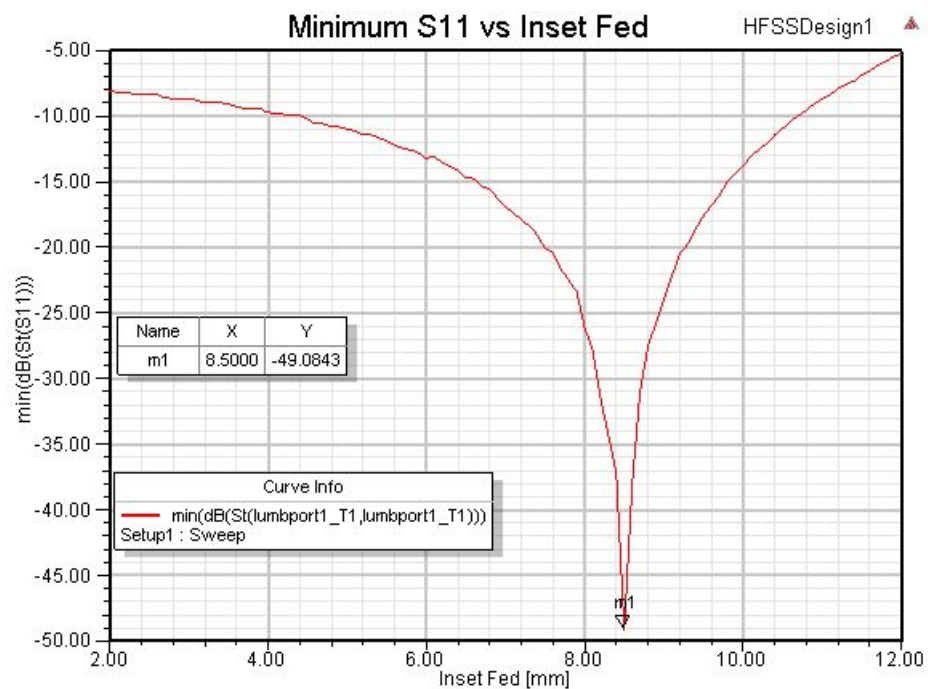


Figure 5.5 The minimum  $S_{11}$  of the patch antenna versus inset-fed length

Additionally, the minimum values of  $S_{11}$  parameter of the patch antenna have been determined for each frequency sweep simulation by searching the frequency response of the patch antenna. The minimum values of  $S_{11}$  parameter have been plotted with respect to the frequency as shown in Figure (5.6).

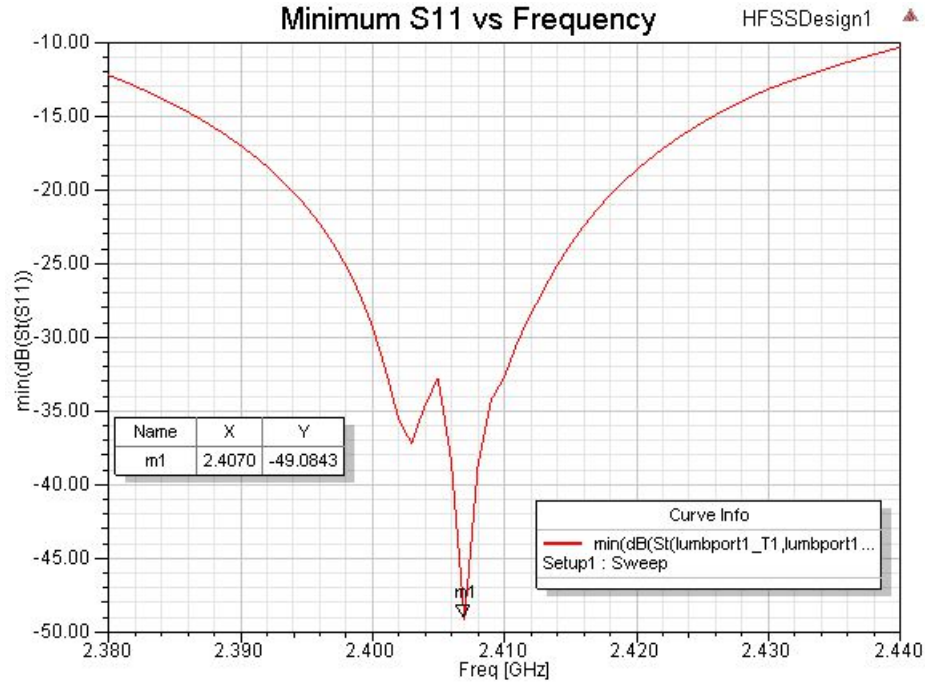


Figure 5.6 The minimum  $S_{11}$  of the patch antenna versus frequency

From Figure (5.4) and Figure (5.5) it has been observed that the matching between the patch antenna and the microstrip line has been provided when the  $L_{if}$  has been equal to 8.5 mm. Likewise, it has been observed from Figure (5.6) that the minimum value of the  $S_{11}$  parameter has been reached at frequency of about 2.41 GHz.

As a result, the patch antenna geometry parameters have been optimized to meet the design specifications. The optimized antenna geometry parameters have been given in Table (5.2). The VSWR and  $S_{11}$  parameter of the patch antenna at  $L_{if} = 8.5$  mm have been plotted with respect to frequency in Figure (5.7) and Figure (5.8), respectively.

Table 5.2 The basic antenna parameters obtained by ANSYS HFSS

Inset-fed microstrip patch antenna parameters				
$W$ (mm)	$L$ (mm)	$L_{if}$ (mm)	$W_0$ (mm)	$W_g$ (mm)
38.02	29.46	8.5	3.02	1.51

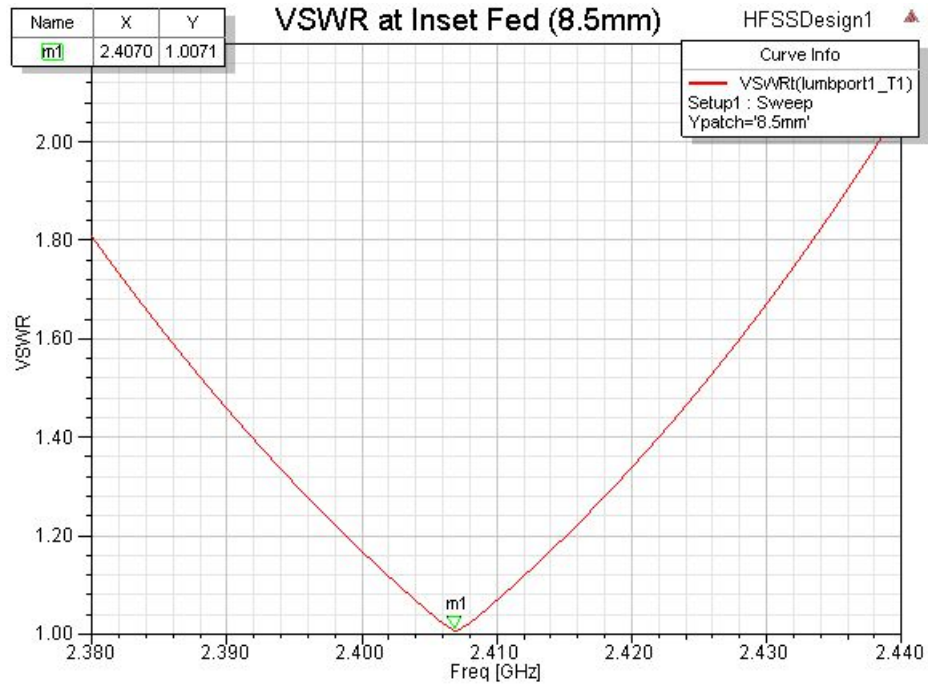


Figure 5.7 The VSWR of patch antenna versus frequency at  $L_{if} = 8.5$  mm

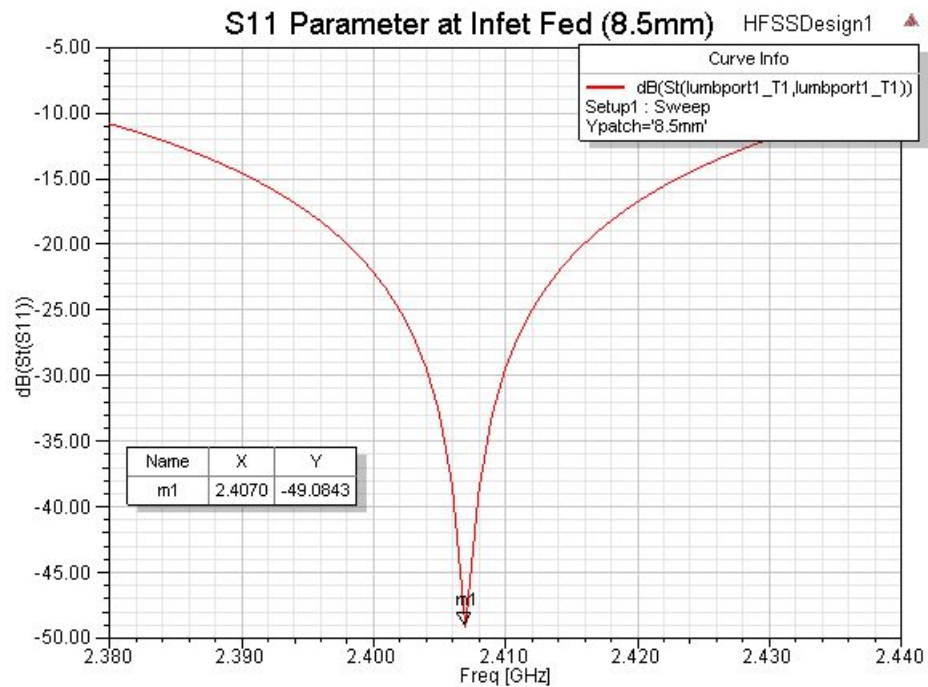


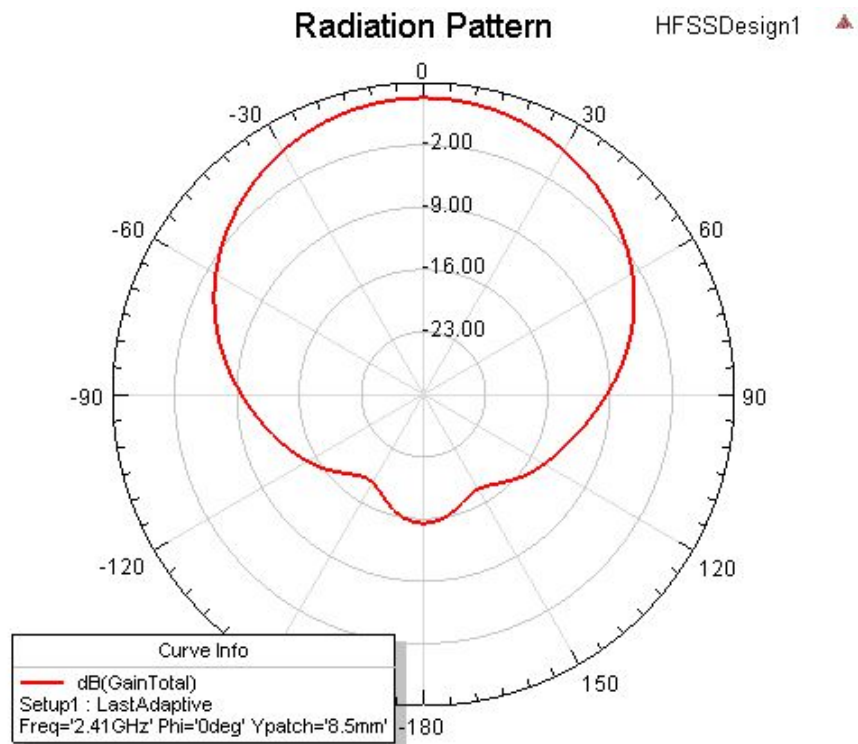
Figure 5.8 The  $S_{11}$  parameter of patch antenna versus frequency at  $L_{if} = 8.5$  mm



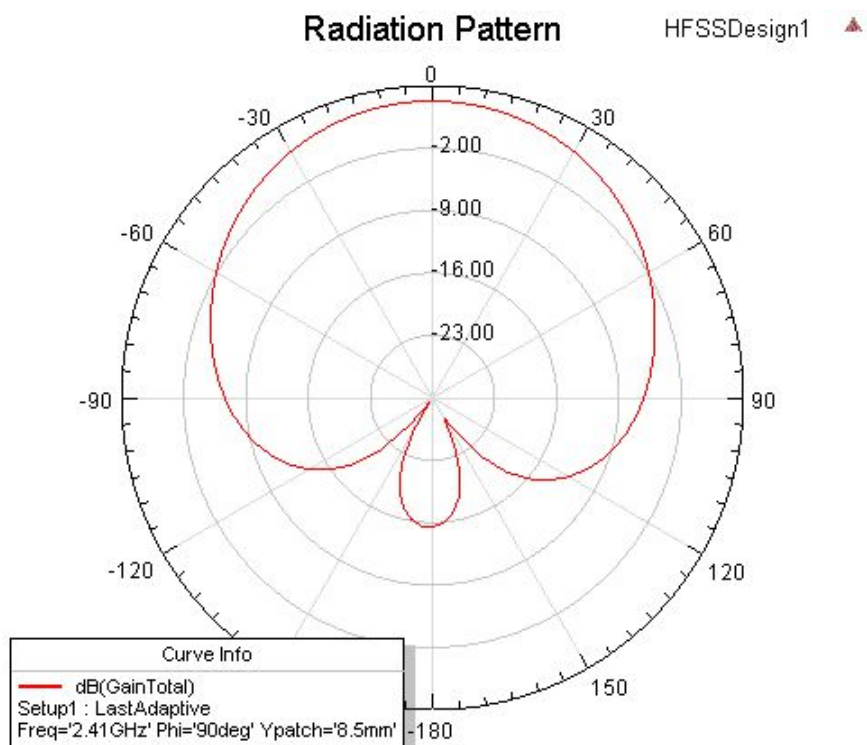
The electrical properties of the designed inset-fed microstrip patch antenna have been computed using ANSYS HFSS software. The results have been given in Table (5.3). The radiation pattern of the patch antenna has been plotted for  $\phi = 0^\circ$  and  $\phi = 90^\circ$  in Figure (5.9). The 3D radiation pattern of the patch antenna has been shown in Figure (5.3b) and Figure (5.3c).

Table 5.3 The electrical properties of the inset-fed patch antenna computed by ANSYS HFSS

Inset-fed microstrip patch antenna parameters	
Peak Directivity	4.8877
Peak Gain ( <i>dB</i> )	2.1429
Peak Realized Gain ( <i>dB</i> )	2.1405
Radiated Power ( <i>mW</i> )	4.379
Accepted Power ( <i>mW</i> )	9.998
Incident Power ( <i>mW</i> )	10
Radiation Efficiency	0.438



(a) Radiation pattern for  $\phi = 0^\circ$



(b) Radiation pattern for  $\phi = 90^\circ$

Figure 5.9 The radiation pattern of the patch antenna

### 5.1.2 Inset-Fed Microstrip Patch Antenna Array

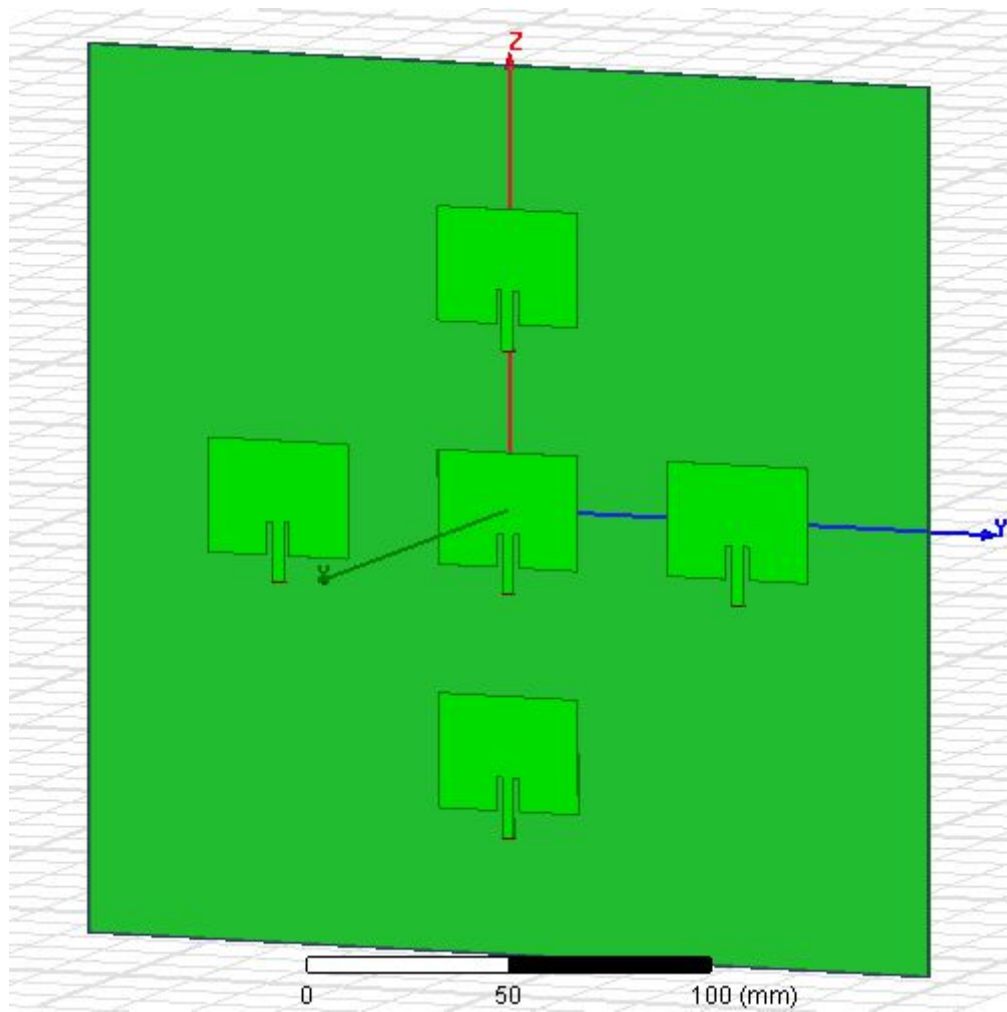
The radio source positioning system needs an antenna array to obtain the azimuth and elevation angles by using direction of arrival of the impinging signal. An inset-fed microstrip patch antenna array has been constructed by using the patch antenna which has been designed in Section (5.1.1). The patch antenna array has been formed using two ULAs which is oriented along y and z axes as shown in Figure (5.10a).

The ANSYS HFSS model has been constructed to examine performance of the inset-fed microstrip patch antenna array. The frequency sweep simulation has been performed to observe the S-parameters of the patch array with respect to frequency. The S-parameters of the each patch antenna in antenna array system are shown in Figure (5.12). It has been observed that The resonant frequency of the patch antennas have slightly deviated and also, value of the  $S_{11}$ -parameters of the patch antennas have slightly increased. However, these changes are within the acceptable range of design specifications.

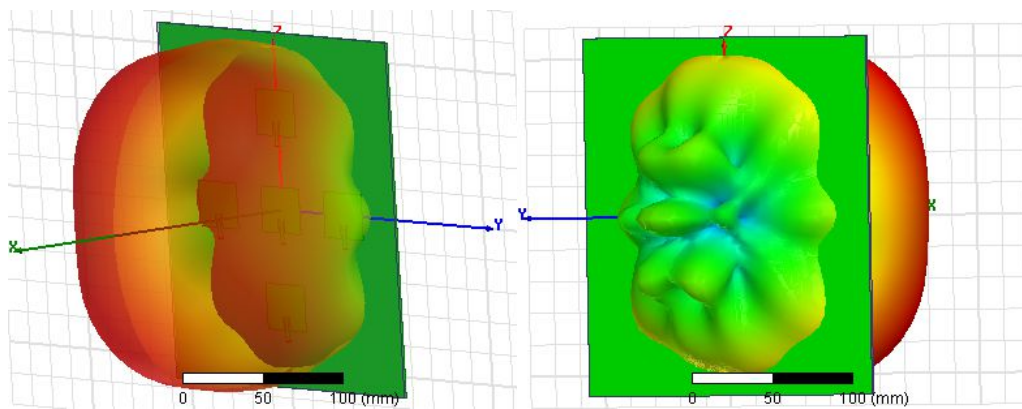
The electrical properties of the designed inset-fed microstrip patch antenna array have been computed using ANSYS HFSS software. The results are given in Table (5.4). The radiation patterns of the patch antenna have been plotted for  $\phi = 0^\circ$  and  $\phi = 90^\circ$  in Figure (5.11). The 3D radiation pattern of the patch antenna has been shown in Figure(5.10b) and Figure (5.10c).

Table 5.4 The electrical properties of the patch antenna array computed by ANSYS HFSS

Inset-fed microstrip patch antenna array parameters	
Peak Directivity	3.9453
Peak Gain (dB)	1.602
Peak Realized Gain (dB)	1.5769
Radiated Power (mW)	3.997
Accepted Power (mW)	9.8443
Incident Power (mW)	10
Radiation Efficiency	0.406



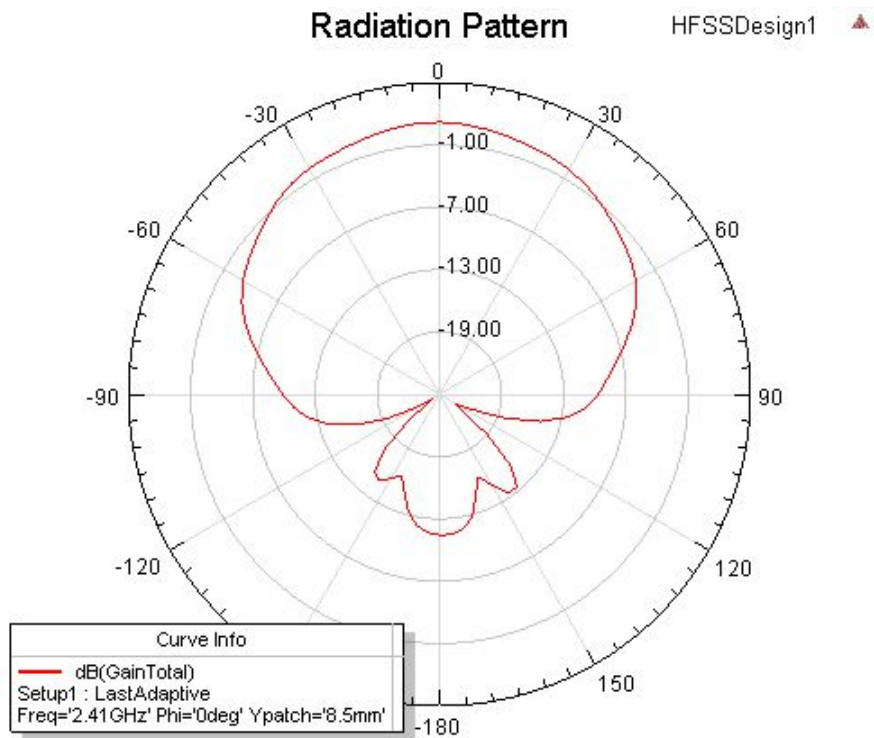
(a) Inset-fed microstrip patch antenna array



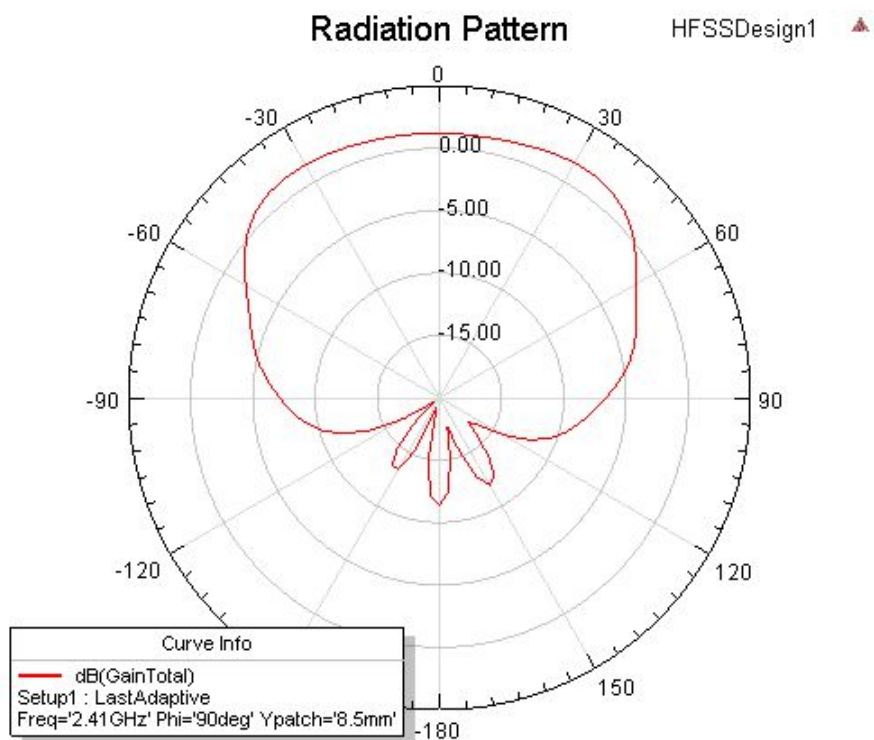
(b) 3D radiation pattern (front)

(c) 3D radiation pattern (back)

Figure 5.10 The inset-fed microstrip patch antenna array



(a) Radiation pattern for  $\phi = 0^\circ$



(b) Radiation pattern for  $\phi = 90^\circ$

Figure 5.11 The radiation pattern of the patch antenna

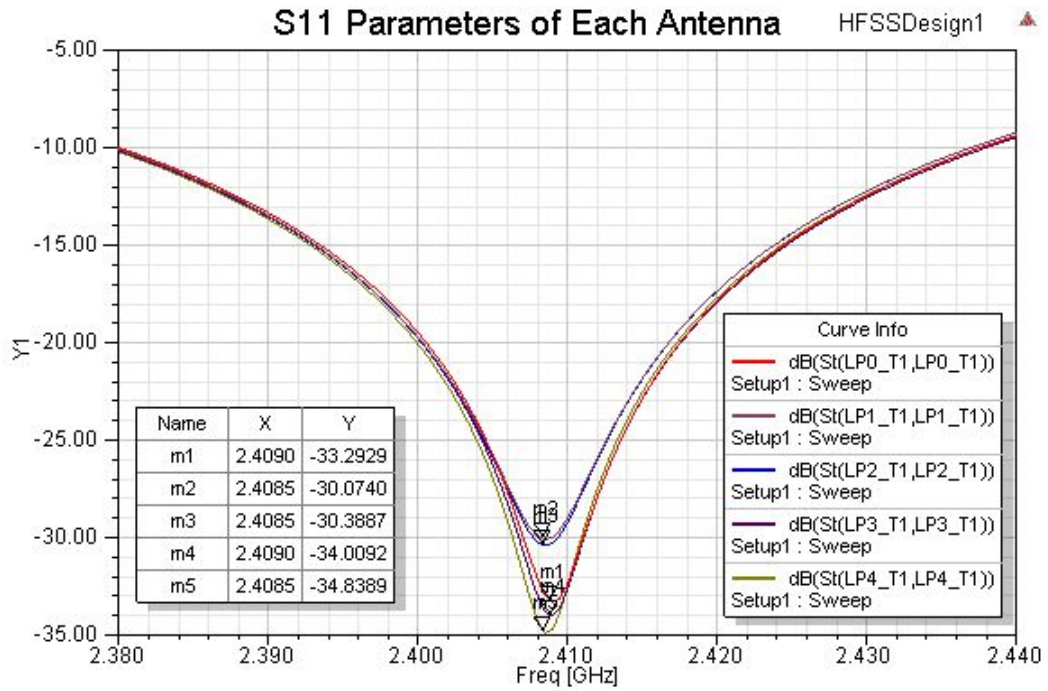


Figure 5.12 The S-parameters of the each patch antenna in antenna array system versus frequency

## 5.2 Chebyshev Bandpass Filter Design

A Chebyshev bandpass filter has been designed using filter design tool of the ANSYS DESIGNER software. The filter has been used for transmission of the signal whose frequency is at the resonant frequency of the inset-fed microstript patch antenna and suppression of the frequencies except the resonant frequency.

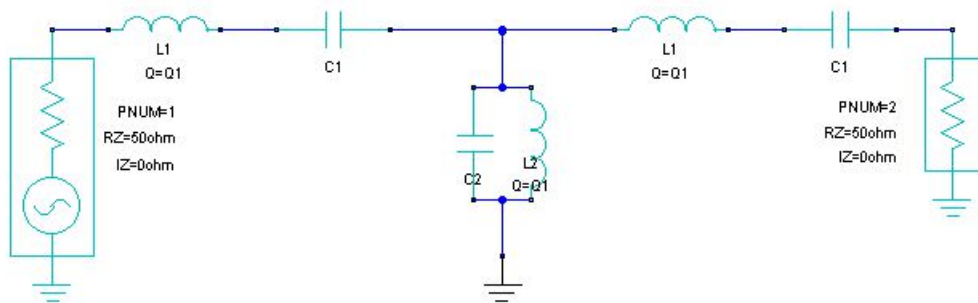


Figure 5.13 The design of the 3<sup>rd</sup> order Chebyshev bandpass filter

The design specifications of the Chebyshev bandpass filter have been chosen as the center frequency of the filter is 2.41 GHz, the bandwidth is 100 MHz, the order of

the filter is 3, the maximum ripple in passband is 0.01 *dB*. Also, the input and output port of the filter has been matched the 50 *Ohm* source impedance and the 50 *Ohm* load impedance, respectively. The filter has been implemented by using the lumped components as shown in Figure (5.13). The values of the lumped components have been given in Table (5.5).

Table 5.5 The values of the lumped components of the designed Chebyshev filter

$L_1$ (nH)	$L_2$ (nH)	$C_1$ (pF)	$C_2$ (pF)
50.06	0.14	0.087	30.885

The performance of the 3<sup>rd</sup> order Chebyshev bandpass filter has been examined by ANSYS DESIGNER. A frequency sweep simulation has been performed between the frequencies 1.8 *GHz* upto 3 *GHz*. The frequency response of the filter has been shown in Figure (5.14)

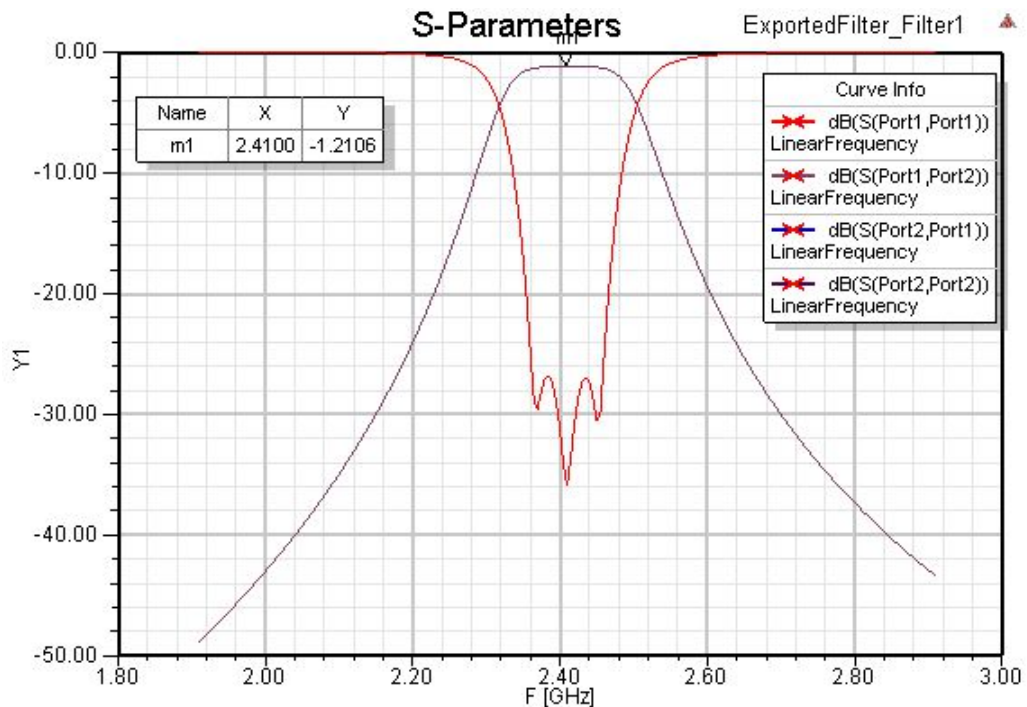


Figure 5.14 The frequency response of the 3<sup>rd</sup> order Chebyshev bandpass filter



### 5.3 RF Driver Amplifier Design

The output signal power of the quadrature modulator is not enough to properly drive the inset-fed patch antenna. Thus, power of the quadrature modulated signal is needed to be amplified. An RF driver amplifier has been designed using the ADL5320 RF driver amplifier IC. The RF input and output of the ADL5320 IC has been matched to the 50  $\Omega$  source impedance and load impedance to increase the performance of the RF driver amplifier. The schematic of the RF driver amplifier design which consists of the source and load matching network has been shown in Figure (5.15).

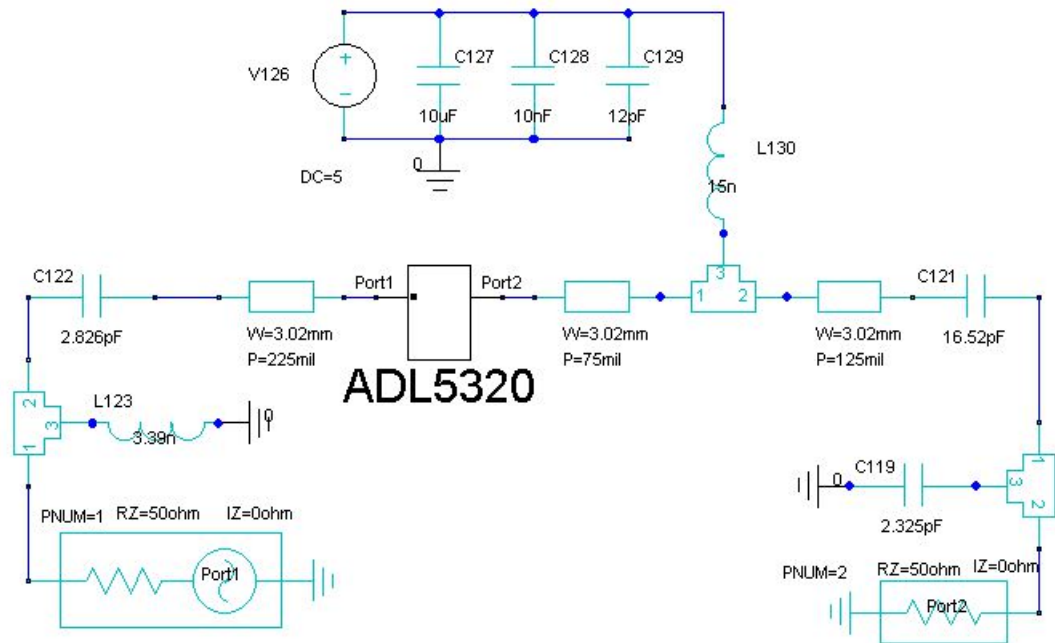


Figure 5.15 The schematic of the RF driver amplifier design

The performance of the RF driver amplifier has been examined using ANSYS DESIGNER software. A frequency sweep simulation has been performed between the frequencies 2.2  $GHz$  upto 2.6  $GHz$ . The frequency response of the designed driver amplifier has been shown in Figure (5.16). From Figure (5.16), it has been observed that the matching of the input and output ports of the RF driver amplifier to the source and load impedance at 2.41  $GHz$  have been provided.



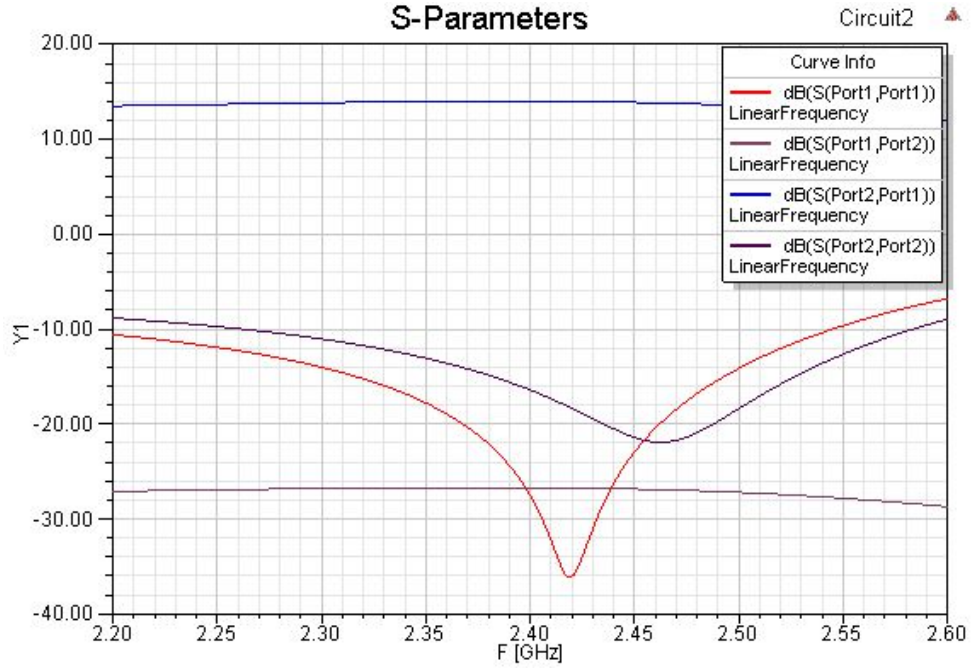


Figure 5.16 The S-parameters of the RF driver amplifier

Additionally, the power gain (GP), available gain (GA) and transducer power gain (GT) of the amplifier (Pozar, 2005) have been investigated. The GP, GA and GT of the designed amplifier have been plotted with respect to frequency as shown in Figure (5.17). Also, it has been seen from Figure (5.17) that the input and output ports of the RF driver amplifier have been matched to the source and load impedance at 2.41 GHz.

### 5.3.1 RF Driver Amplifier with Bandpass Filter

The common behavior of the RF driver amplifier and the Chebyshev bandpass filter has been examined. A frequency sweep simulation has been performed between the frequencies 2.2 GHz and 2.6 GHz. The frequency response of the combined system has been shown in Figure (5.18). Also, the GP, GA and GT of the combined system have been plotted with respect to frequency as shown in Figure (5.19).

It has been seen from Figure (5.18) and Figure (5.19) that the common behavior of the RF driver amplifier and the Chebyshev bandpass filter is suitable to work with the inset-fed microstrip patch antenna. Hence, the RF front-end of the transmitter unit

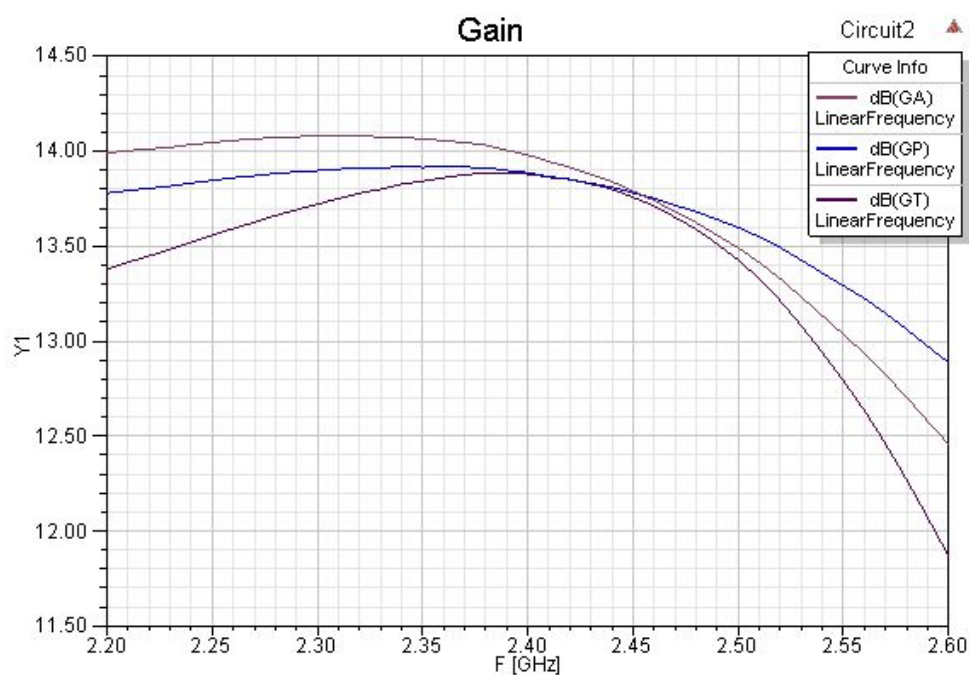


Figure 5.17 The GP, GA and GT of the amplifier w.r.t. frequency

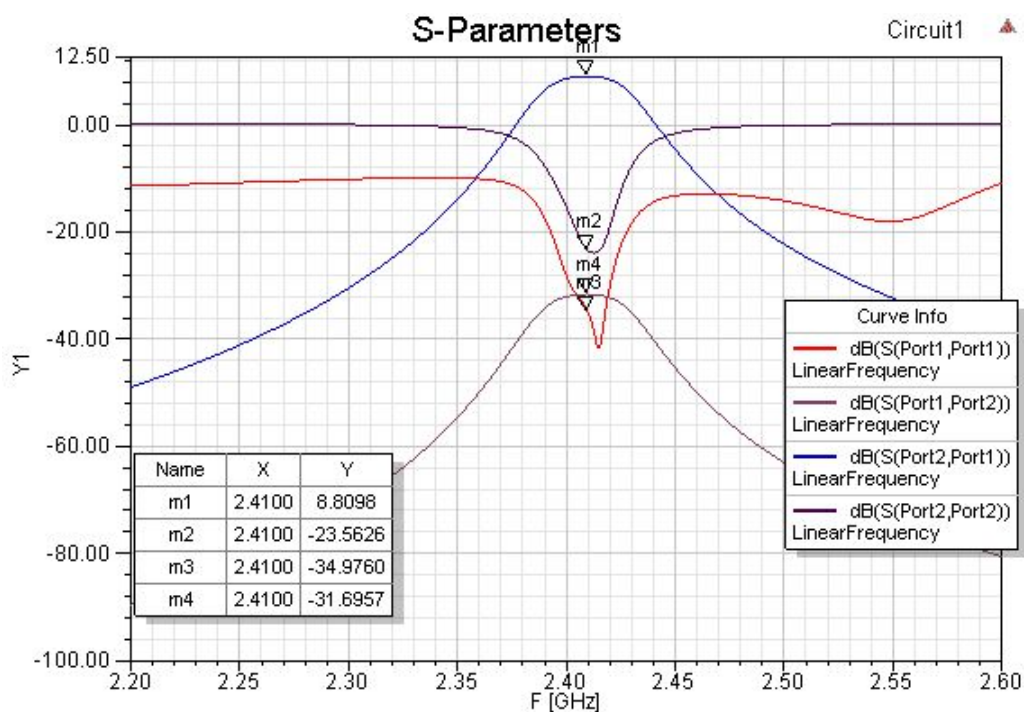


Figure 5.18 The frequency response of the RF driver amplifier together with the bandpass filter

(radio source) has been accomplished successfully.

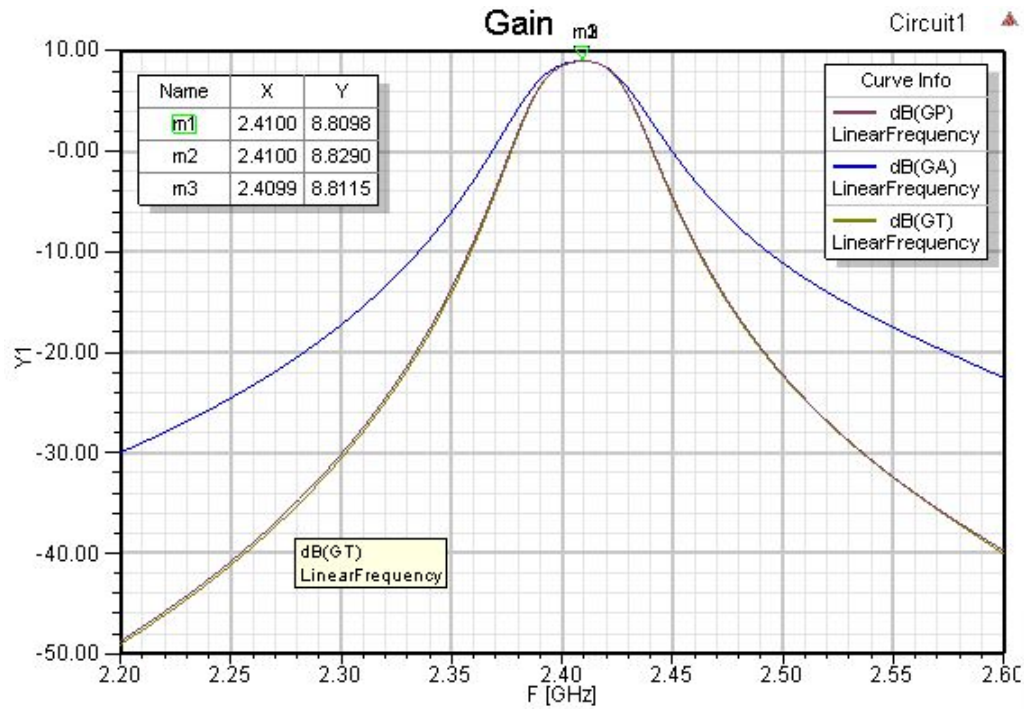


Figure 5.19 the GP, GA and GT of the combined system w.r.t frequency

#### 5.4 Low Noise Amplifier Design

The quadrature modulated signal received by the inset-fed microstrip patch antenna is weak. Thus, power of the received signal has been needed to be amplified before the quadrature demodulation of signal. A low noise amplifier has been designed using the ADL5523 low noise amplifier IC as shown in Figure (5.20).

The performance of the low noise amplifier has been examined using ANSYS DESIGNER software. A frequency sweep simulation has been performed between the frequencies 2 GHz up to 2.8 GHz. The frequency response of the low noise amplifier has been shown in Figure (5.21). Also, the GP, GA and GT of the low noise amplifier have been plotted with respect to frequency as shown in Figure (5.22).

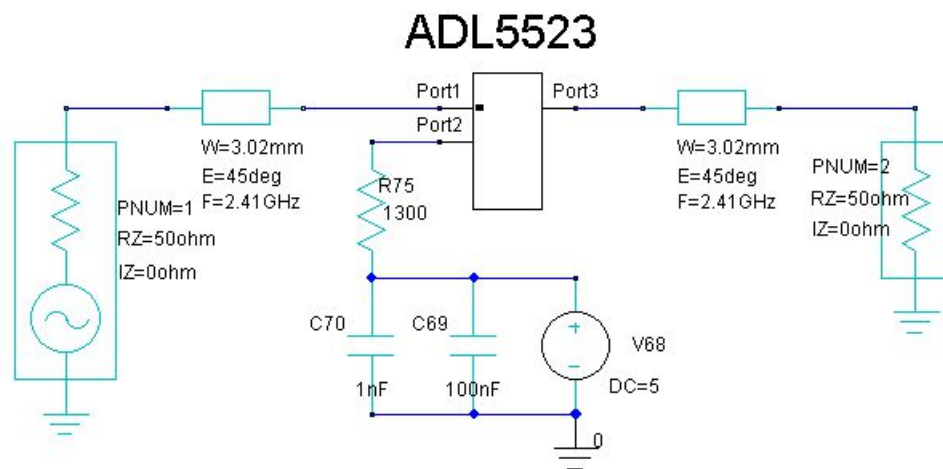


Figure 5.20 The schematic of the low noise amplifier design

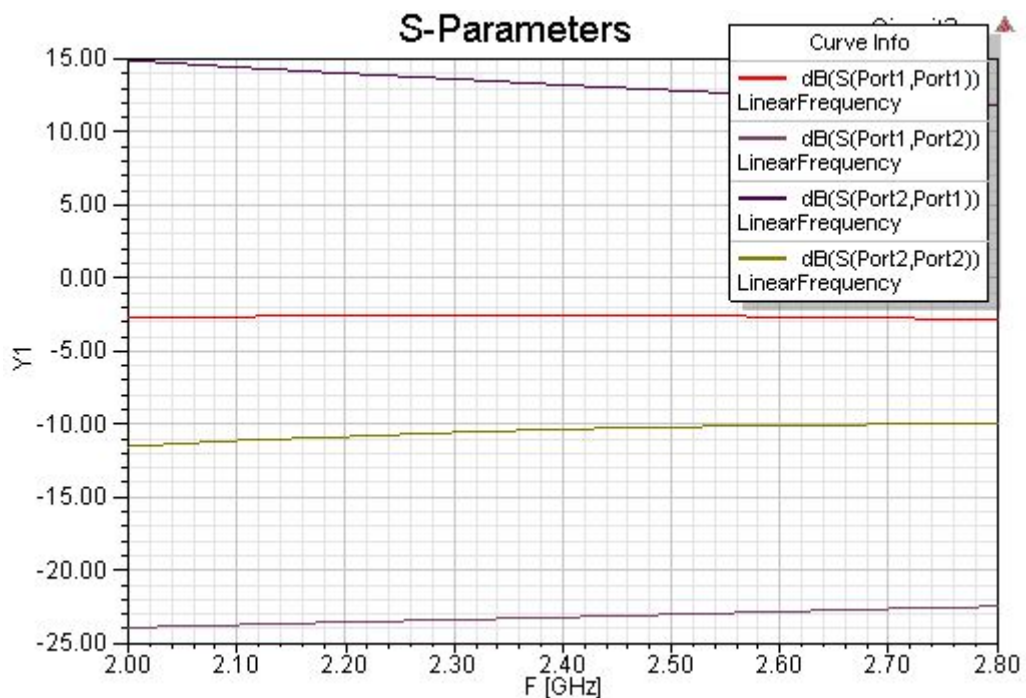


Figure 5.21 The frequency response of the low noise amplifier

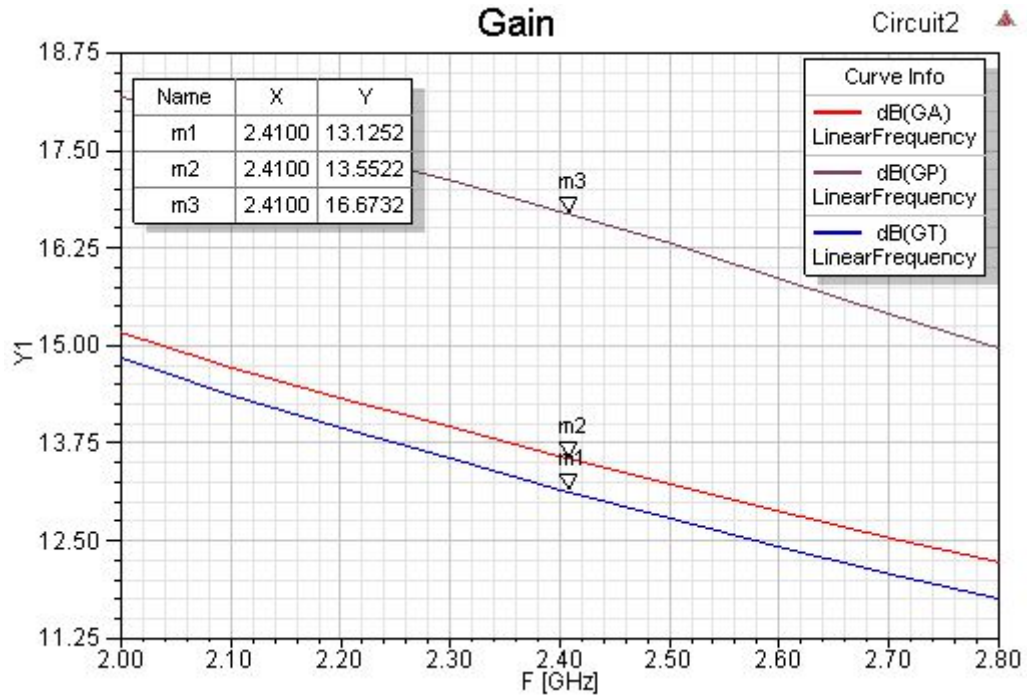


Figure 5.22 The GP, GA and GT of the low noise amplifier w.r.t. frequency

#### 5.4.1 Low Noise Amplifier with Bandpass Filter

The common behavior of the low noise amplifier and the Chebyshev bandpass filter has been examined. A frequency sweep simulation has been performed between the frequencies  $2.2\text{ GHz}$  upto  $2.6\text{ GHz}$ . The frequency response of the combined system has been shown in Figure (5.23). Also, the GP, GA and GT of the combined system has been plotted with respect to frequency as shown in Figure (5.24).

It has been seen from Figure (5.23) and Figure (5.24) that the common behavior of the RF driver amplifier and the Chebyshev bandpass filter is suitable to work with the inset-fed microstrip patch antenna. Hence, the RF front-end of the receiver unit (local node) has been accomplished successfully.



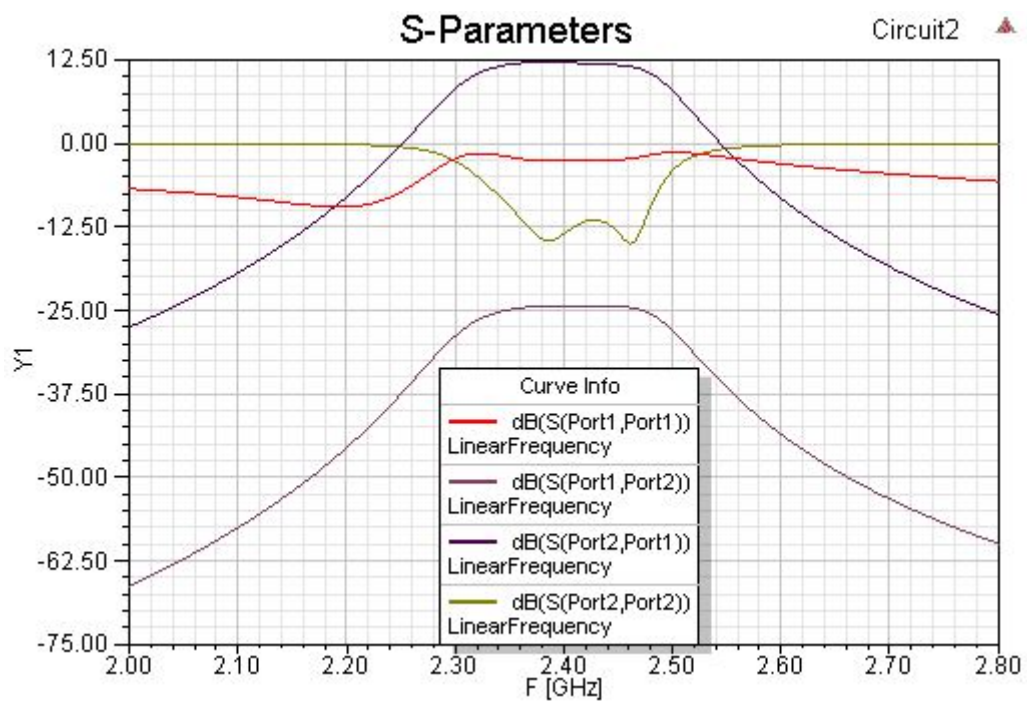


Figure 5.23 The frequency response of the RF driver amplifier together with the bandpass filter

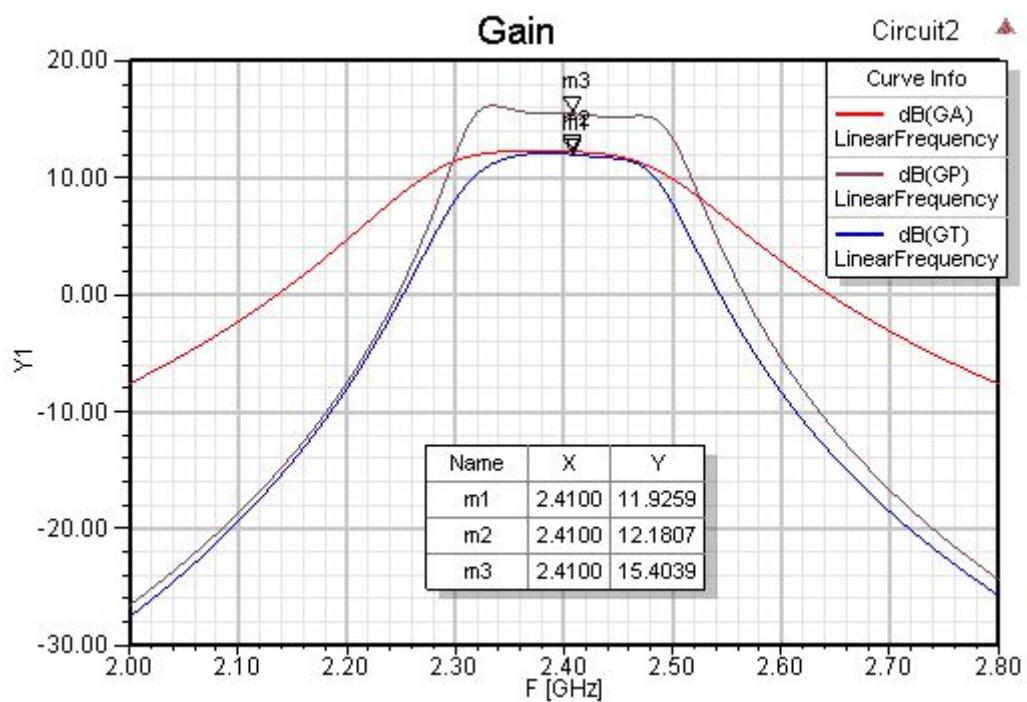


Figure 5.24 the GP, GA and GT of the combined system w.r.t frequency

## CHAPTER SIX

### SIMULATIONS AND PERFORMANCE ASSESSMENT

A Matlab<sup>TM</sup> based simulation software has been developed to examine performance of the radio source positioning system. The basic software architecture is that the complex baseband signal is modulated using the analog QAM technique as in (2.15). It has been assumed that, the modulated signal radiates and propagates from a point in 3-D space through the AWGN channel and arrives at the antenna array system on reference node and local nodes whose locations in 3-D space are known precisely. The antenna array system receives the impinging signal in each node. The received signals have been demodulated and the observation matrix shown in (3.7) is obtained for the ULA systems oriented along the y-axis and z-axis in a node. The MUSIC algorithm has been used to obtain the azimuth and elevation angles with respect to their local coordinate systems in each node. The positioning algorithm has been executed to calculate the position of the radio source in 3-D space. The system of linear equations (4.53) has been obtained by using the azimuth and the elevation angles and the nodes' rotation and translation information. The position of the source signal is determined by solving (4.53).

The position estimation error is calculated to examine performance. The DoA estimation error is assumed to have Gaussian probability density function as a result of the MUSIC algorithm. Hence, the estimation error of the  $x, y, z$  coordinates is also assumed to have Gaussian probability density function. The position estimation error is defined as,

$$P_{error} = \sqrt{(3\sigma_x)^2 + (3\sigma_y)^2 + (3\sigma_z)^2} \quad (6.1)$$

where  $\sigma_x, \sigma_y, \sigma_z$  are standard deviation of  $E[x], E[y], E[z]$  coordinates, respectively. The standard deviation has been estimated using 1000 samples. In each process a AWGN has been randomly generated according to a specified signal to noise ratio (SNR),

$$SNR_{dB} = 10 \log \left( \frac{P_{signal}}{P_{noise}} \right) \quad (6.2)$$

where  $P_{signal}$  is average signal power and  $P_{noise}$  is average noise power.

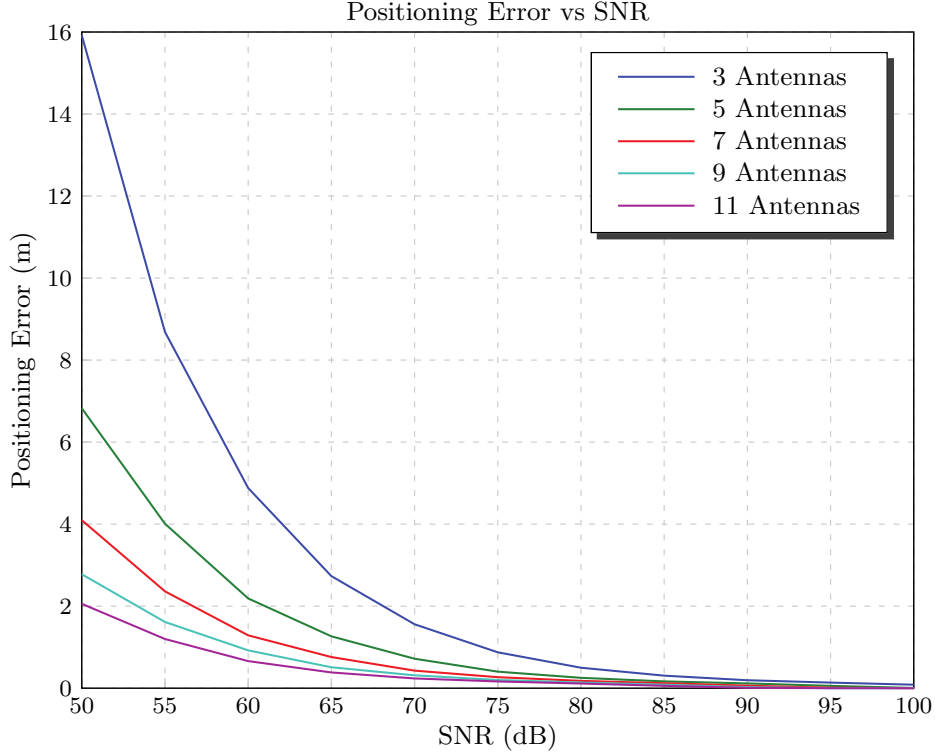


Figure 6.1 The position estimation error versus SNR. QAM signal carrier frequency is 2.4 GHz

Table 6.1 The position estimation error versus SNR with respect to number of antenna elements. QAM signal carrier frequency is 2.4 GHz

# of Antennas	SNR (dB)											Positioning Error (m)
	50	55	60	65	70	75	80	85	90	95	100	
3 Antennas	15.9	8.68	4.88	2.73	1.56	0.87	0.5	0.31	0.19	0.14	0.08	
5 Antennas	6.83	4.00	2.19	1.26	0.72	0.40	0.25	0.16	0.12	0.06	0.01	
7 Antennas	4.09	2.36	1.29	0.76	0.43	0.27	0.18	0.12	0.06	0.01	.001	
9 Antennas	2.77	1.61	0.92	0.51	0.31	0.2	0.14	0.09	0.03	.001	.001	
11 Antennas	2.05	1.2	0.66	0.38	0.24	0.16	0.11	0.06	.008	.001	.001	

The position estimation error of the radio source positioning system has been examined with respect to SNR and then the effect of the number of the antennas in the ULA system has been considered. The results of the simulation are shown in Figure (6.1) and given in Table (6.1). The complex baseband signal frequency  $f_0$  is 1 MHz and the carrier frequency of QAM signal  $f_c$  is 2.4 GHz. The reference node  $R$  is located in position (0,0,0) and the local nodes  $N_1$  and  $N_2$  are located in positions (50,50,-5) and (50,-50,10), respectively. The  $N_1$  rotation angles are  $\gamma = -70$ ,  $\beta = 0$



and  $\alpha = 0$  with respect to the  $R$ . The  $N_2$  rotation angles are  $\gamma = 75$ ,  $\beta = 0$  and  $\alpha = 0$  with respect to the  $R$ . The exact position of the radio source has been randomly chosen as  $(40, -20, -25)$ . The noise has been assumed to be AWGN.

The above simulation has been repeated to observe the effect of the carrier frequency to positioning error. This time, the carrier frequency of QAM signal  $f_c$  is  $1\text{ GHz}$ . The results of the simulation are shown in Figure (6.2) and given in Table (6.2).

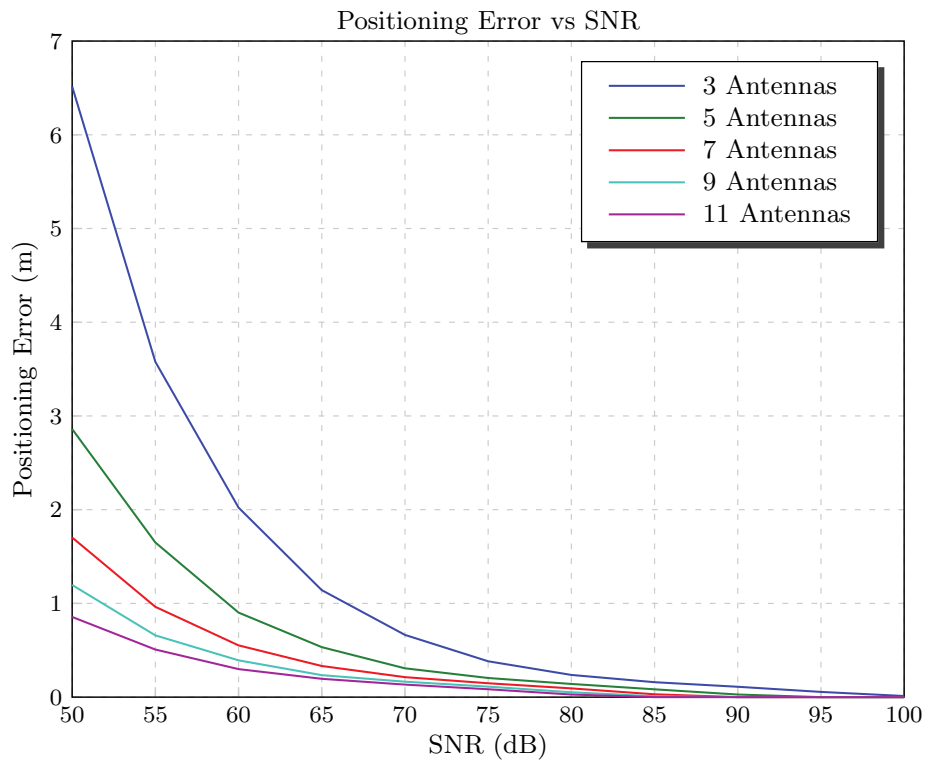


Figure 6.2 The position estimation error versus SNR. QAM signal carrier frequency is  $1\text{ GHz}$

Table 6.2 The position estimation error versus signal to noise ratio with respect to number of antenna elements. QAM signal carrier frequency is  $1\text{ GHz}$

	SNR (dB)											
# of Antennas	50	55	60	65	70	75	80	85	90	95	100	Positioning Error (m)
3 Antennas	6.5	3.58	2.02	1.14	0.66	0.38	0.24	0.16	0.11	0.05	0.01	
5 Antennas	2.86	1.65	0.90	0.53	0.31	0.20	0.14	0.08	0.03	.001	.001	
7 Antennas	1.7	0.96	0.55	0.33	0.21	0.15	0.09	0.03	.001	.001	.001	
9 Antennas	1.19	0.66	0.39	0.23	0.16	0.11	.05	.009	.001	.001	.001	
11 Antennas	0.86	0.51	0.30	0.20	0.13	0.08	.02	.001	.001	.001	.001	

The effect of the SNR value on positioning process can be roughly seen from Figure (6.1) and Figure (6.2). The position estimation error decreases, when the SNR value increases. The number of the antenna elements in a ULA antenna system has positive effect. The position estimation results becomes better, when the number of the antenna elements are increased. The reason of the enhancement is that the number of the eigenvectors which defines the noise subspace increases, as a result the performance of the MUSIC algorithm increases. Hence, the estimation error of the azimuth and the elevation angles decrease. When Figure (6.1) and Figure (6.2) are compared, it is seen that variation in carrier frequency of QAM signal has effect on position estimation error. The results of positioning system whose carrier frequency is 1 GHz is better than the results of positioning system whose carrier frequency is 2.4 GHz.

The position estimation error of the radio source positioning system has been examined with respect to the carrier frequency of QAM signal and also, the effect of the number of the antennas in the ULA system has been observed. The results of the simulation have been shown in Figure (6.3) and given in Table (6.3). The complex baseband signal frequency  $f_0$  is 1 MHz. The reference node  $R$  is located in position (0,0,0) and the local nodes  $N_1$  and  $N_2$  are located in positions (50,50,-5) and (50,-50,10), respectively.  $N_1$  rotation angles are  $\gamma = -70$ ,  $\beta = 0$  and  $\alpha = 0$  with respect to the  $R$ .  $N_2$  rotation angles are  $\gamma = 75$ ,  $\beta = 0$  and  $\alpha = 0$  with respect to the  $R$ . The exact position of the radio source is (40,10,-5). The SNR value is 60 dB. The noise effecting the channel and the antenna array system has been assumed to be AWGN.

The effect of the carrier frequency of QAM signal during positioning process can be investigated from Figure (6.3) and Table (6.3). The position estimation error increases, when the carrier frequency increases. Here, decreasing the carrier frequency of signal can be a good choice. However, decreasing the carrier frequency increases the physical size of the antennas and also physical size of the overall system. The distance between the antenna elements on ULA also increases. However, the position estimation error decreases inversely proportional to the carrier frequency

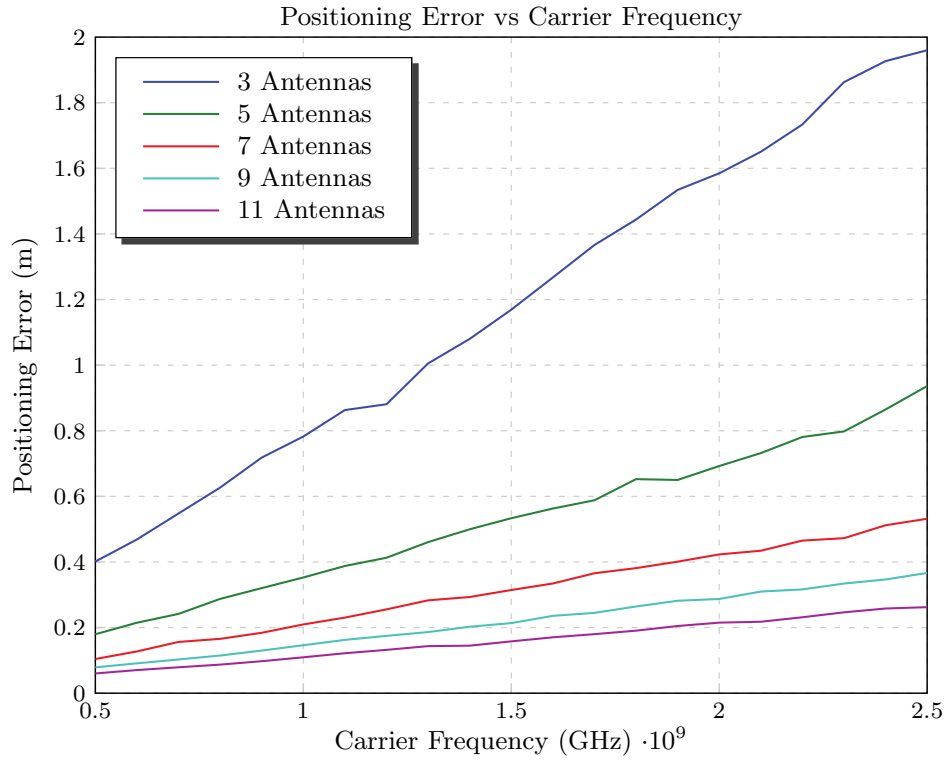


Figure 6.3 The position estimation error versus carrier frequency

of QAM signal. The reason of the enhancement is that distance between antenna

Table 6.3 The position estimation error versus carrier frequency with respect to number of antenna elements

	Frequency (GHz)											
# of Antennas	0.5	0.7	0.9	1.1	1.3	1.5	1.7	1.9	2.1	2.3	2.5	Positioning Error (m)
3 Antennas	0.40	0.54	0.72	0.86	1.00	1.17	1.37	1.53	1.65	1.86	1.96	
5 Antennas	0.18	0.24	0.32	0.39	0.46	0.53	0.58	0.65	0.73	0.80	0.94	
7 Antennas	0.10	0.16	0.18	0.23	0.28	0.31	0.37	0.40	0.43	0.47	0.53	
9 Antennas	0.08	0.10	0.13	0.16	0.18	0.21	0.24	0.28	0.31	0.33	0.37	
11 Antennas	0.06	0.08	0.10	0.12	0.14	0.16	0.18	0.20	0.22	0.25	0.26	

elements is related to the wavelength of the carrier signal and the ratio between the carrier signal wavelength and baseband wavelength has effect on resolution of the DoA estimation. When the carrier wavelength is too small with respect to the baseband signal wavelength, the resolution of the DoA estimation decreases. Therefore, the effect of the SNR increases on position estimation process. This is recognizable when Figure (6.1) and Figure (6.2) are compared. As in the SNR test

results, the number of the elements in a ULA antenna system has positive effect. The position estimation results are enhanced, when the number of the antenna elements are increased.

## 6.1 Trajectory Tracking

The trajectory of an object traveling in 3-D space has been tracked with the radio source positioning system. The tracking process has been simulated and the positioning errors have been measured during the tracking process. The results of the simulation is shown in Figure (6.4) and given in Table (6.4). The complex baseband signal frequency  $f_0$  is 1 MHz and carrier frequency  $f_c$  is 2.4 GHz. The number of the antennas in a ULA is 3. The reference node  $R$  is located in position (0,0,0) and the local nodes  $N_1$  and  $N_2$  are located in positions (50,50,-5) and (50,-50,10), respectively. The  $N_1$  rotation angles are  $\gamma = -70$ ,  $\beta = 0$  and  $\alpha = 0$  with respect to the  $R$ . The  $N_2$  rotation angles are  $\gamma = 75$ ,  $\beta = 0$  and  $\alpha = 0$  with respect to the  $R$ . The SNR value is 60 dB. The noise effecting the channel and the antenna array system has been assumed to be AWGN.

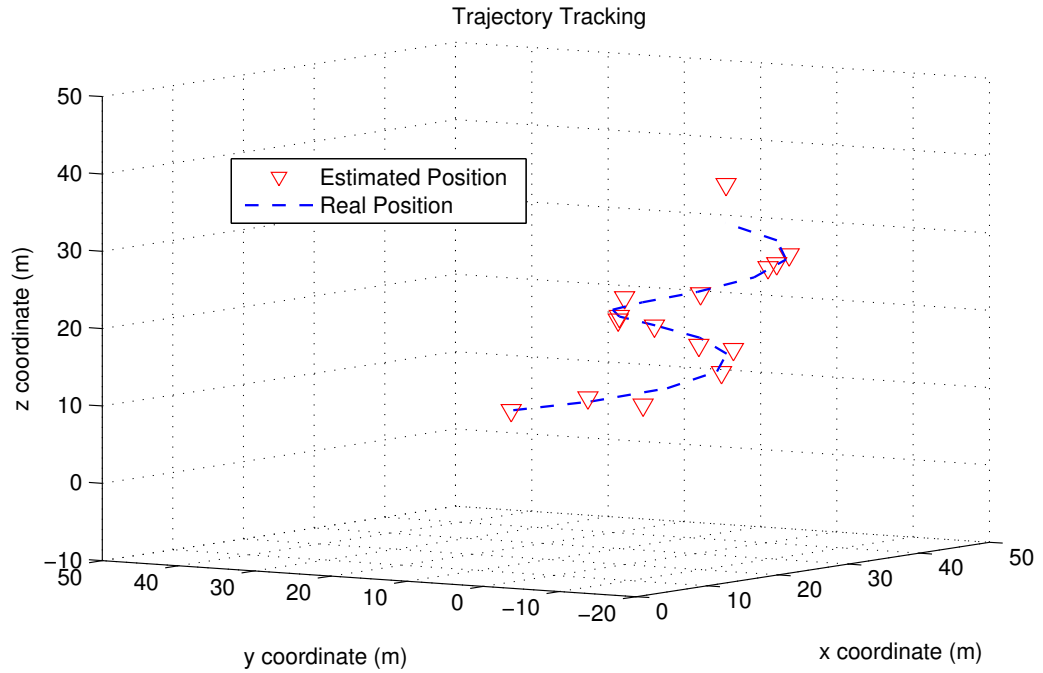


Figure 6.4 The trajectory tracking with positioning system designed with 3 element antenna array system

Table 6.4 The trajectory tracking with positioning system designed with 3 element antenna array system

<b>Number</b>	<b>Real Position</b> $(x, y, z)$	<b>Estimated Position</b> $(\tilde{x}, \tilde{y}, \tilde{z})$	<b>Positioning Error</b> (m)
1	(15, 10, 10)	(14.23, 8.48, 8.96)	1.997
2	(16.82, 1.54, 11.43)	(16.45, 1.50, 11.96)	0.649
3	(21.57, -4.09, 12.86)	(23.59, -3.78, 12.81)	2.044
4	(27.39, -5.24, 14.28)	(27.67, -6.18, 15.07)	1.257
5	(32.08, -2.16, 15.71)	(31.39, -1.31, 15.26)	1.177
6	(34.06, 3.21, 17.14)	(33.66, 3.30, 16.57)	0.703
7	(33.01, 8.07, 18.57)	(32.13, 7.24, 18.71)	1.217
8	(30, 10, 20)	(29.38, 8.98, 22.24)	2.537
9	(26.99, 8.07, 21.43)	(26.87, 6.45, 20.68)	1.786
10	(25.94, 3.22, 22.86)	(25.93, 2.95, 21.35)	1.529
11	(27.92, -2.16, 24.28)	(26.71, -2.71, 24.09)	1.34
12	(32.61, -5.24, 25.71)	(31.35, -5.92, 25.37)	1.472
13	(38.43, -4.09, 27.14)	(39.12, -3.90, 25.53)	1.765
14	(43.18, 1.54, 28.57)	(41.37, 0.87, 29.84)	2.308
15	(45, 10, 30)	(45.32, 8.89, 31.15)	1.63

The above simulation has been repeated to observe effect of the number of ULA antenna to positioning error during the tracking process. This time, the number of the antennas in a ULA is 5. The results of the simulation are shown in Figure (6.5) and given in Table (6.5).

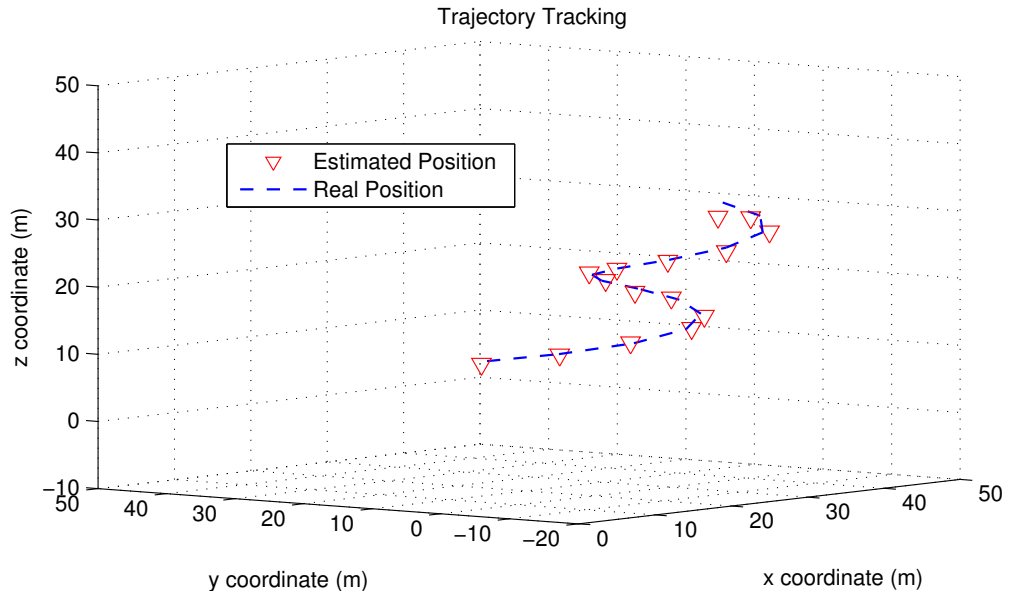


Figure 6.5 The trajectory tracking with positioning system designed with 5 element antenna array system

Table 6.5 The trajectory tracking with positioning system designed with 5 element antenna array system

Number	Real Position ( $x, y, z$ )	Estimated Position ( $\tilde{x}, \tilde{y}, \tilde{z}$ )	Positioning Error (m)
1	(15, 10, 10)	(14.83, 9.89, 9.92)	0.213
2	(16.82, 1.54, 11.43)	(17.03, 1.55, 12.02)	0.627
3	(21.57, -4.09, 12.86)	(22.58, -4.72, 13.32)	1.280
4	(27.39, -5.24, 14.28)	(27.59, -4.72, 14.39)	0.575
5	(32.08, -2.16, 15.71)	(32.18, -2.42, 15.74)	0.283
6	(34.06, 3.21, 17.14)	(34.53, 2.47, 17.04)	0.887
7	(33.01, 8.07, 18.57)	(33.45, 8.09, 18.76)	0.478
8	(30, 10, 20)	(29.77, 10.42, 19.78)	0.530
9	(26.99, 8.07, 21.43)	(26.77, 7.52, 21.57)	0.606
10	(25.94, 3.22, 22.86)	(24.85, 3.32, 22.34)	1.207
11	(27.92, -2.16, 24.28)	(27.93, -1.90, 24.51)	0.337
12	(32.61, -5.24, 25.71)	(32.38, -4.72, 25.29)	0.706
13	(38.43, -4.09, 27.14)	(38.58, -4.12, 26.66)	0.502
14	(43.18, 1.54, 28.57)	(43.26, 1.43, 28.32)	0.281
15	(45, 10, 30)	(44.71, 10.32, 28.45)	1.607

## CHAPTER SEVEN

### CONCLUSION

An active positioning system has been designed that determines the position of multiple radio sources, produce and emit the QAM signals, in three dimensional space via estimation of direction of arrival. The spectral MUSIC algorithm has been used with the ULA antennas to obtain DoA angles to locate the active radio sources in 3-D space. Two ULA antenna arrays have been oriented along  $y$  and  $z$  axes to obtain the azimuth and the elevation angles and broadside of ULA antenna arrays have been oriented along  $x$  axis on a reference node and local nodes.

The design of radio sources have been done to lower cost and to decrease physical size. The RF front-end of the radio source and the receiver units have been designed using the ANSYS DESIGNER software. The ULA antenna system has been designed using the inset-fed microstrip patch antennas that receive analog QAM signals. The design of inset-fed microstrip patch antennas and performance assessments of the patch antennas have been made using the ANSYS HFSS software. Also, the positioning system's overall cost has been decreased by use of QAM.

The rotation and translation properties of the coordinate transformations have been used to develop a positioning algorithm that solves the 3-D positioning problem. The positioning problem has been reduced to solution of a system of linear equations.

The performance of the radio source positioning system has been examined by the simulation software which is developed on Matlab<sup>TM</sup>. The position estimation error has been used as a criterion to examine the performance of the active radio source positioning system. The effects of the SNR value, number of the antenna elements in a ULA antenna system and the carrier frequency of QAM signal have been investigated. Also, a trajectory of an object traveling in 3-D space has been tracked by using the radio source positioning system.

Consequently, an active positioning system has been developed that identify the location of the radio source in three dimensional space via estimation of the DoA

angles of the radio signals. Also, performance of the radio source positioning system has been examined and effects of the SNR value, number of the antenna elements in a ULA antenna system and the carrier frequency of QAM signal have been investigated. In light of the obtained results it has been seen that the designed positioning system is suitable to be used as a local positioning system that determines an object position in 3-D space with respect to global and local coordinate systems.



## REFERENCES

- Balanis, C. A. (1997). *Antenna theory analysis and design*. United States of America: John Wiley and Sons, Inc.
- Barabell, A. (1983). Improving the resolution of eigenstructure based direction finding algorithms. *Proceedings International Conference on Acoustics, Speech and Signal Processing, Boston, MA*, 336–339.
- DeGroat, R. D., Dowling, E. M., & Linebarger, D. A. (1993). The constrained MUSIC problem. *IEEE Transactions Signal Processing*, 41, 1445–1449.
- El-Behery, I. N., & MacPhie, R. H. (1977). Maximum likelihood estimation of source parameters from time-sampled outputs of a linear array. *The Journal of the Acoustical Society of America*, 62, 1.
- Evans, J., Johnson, J., & Sun, D. (1982). *Application of advanced signal processing techniques to angle of arrival estimation in ATC navigation and surveillance systems*. Technical Report, Massachusetts Institute of Technology.
- Godara, C. (1997a). Applications of antenna arrays to mobile communications, part I: performance improvement, feasibility, and system considerations. *Proceedings of the IEEE*, 85, 7, 1031–1060.
- Godara, C. (1997b). Applications of antenna arrays to mobile communications, part ii: beam-forming and direction-of-arrival considerations. *Proceedings of the IEEE*, 85, 8, 1195–1244.
- Gustafsson, F., & Gunnarsson, F. (2003). Positioning using time-difference of arrival measurements. *IEEE Transactions on Acoustics, Speech, and Signal Processing*, 6, VI – 553–6.
- Hwang, H., Aliyazıcıoğlu, Z., Grice, M., & Yakovlev, A. (2008). Sensitivity analysis for direction of arrival estimation using a root-music algorithm. *Proceedings of the International MultiConference of Engineers and Computer Scientists*, 2.

- John, G. P., & Masoud, S. (2002). *Communication systems engineering*. New Jersey: Prentice Hall.
- Johnson, D. H. (1982). The application of spectral estimation methods to bearing estimation problems. *Proceedings of the IEEE*, 70, 1018–1028.
- Lanzisera, S., Zats, D., & S. J. Pister, K. (2011). Radio frequency time-of-flight distance measurement for low-cost wireless sensor localization. *IEEE Sensors Journal*, 11, 3, 837–845.
- Lee, A., Chen, L., Wei, J., & Hwang, H. (2005). Simulation study of wideband interference rejection using adaptive array antenna. *IEEE Aerospace Conference*.
- Mayhan, J. T., & Niro, L. (1987). Spatial spectral estimation using multiple beam antennas. *IEEE Transactions Antennas Propagation*, AP-35, 897–906.
- Miller, M. I., & Fuhrmann, D. R. (1990). Maximum likelihood narrow-band direction finding and the EM algorithm. *IEEE Transactions Acoustics, Speech, Signal Processing*, 38, 1560–1577.
- Oguejiofor, O., Okorogu, V., Abe, A., & Osuesu, B. (2013). Outdoor localization system using RSSI measurement of wireless sensor network . *International Journal of Innovative Technology and Exploring Engineering*, 2-2.
- Pozar, D. M. (2005). *Microwave engineering*. United States of America: John Wiley and Sons, Inc.
- Rappaport, T. (1991). Wireless personal communications: trends and challenges. *IEEE Antennas Propagation Magazine*, 31, 19–29.
- Roy, R., & Kailath, T. (1989). ESPRIT—Estimation of signal parameters via rotational invariance techniques. *IEEE Transactions Acoustics, Speech, Signal Processing*, ASSP-37, 984–995.
- Schmidt, R. O. (1986). Multiple emitter location and signal parameter estimation. *IEEE Transactions Antennas Propagation*, AP-34, 276–280.

- William, W., & Lajos, H. (1994). *Modern quadrature amplitude modulation principles and applications for fixed and wireless communications*. London: IEEE Press and Pentech Press.
- Zarchan, P. (1996). *Global positioning system: theory and applications volume I*. American Institute of Aeronautics and Astronautics, Inc.
- Zoltowski, M. D., Kautz, G. M., & Silverstein, S. D. (1993a). Beamspace root-MUSIC. *IEEE Transactions Signal Processing*, 41, 344–364.
- Zoltowski, M. D., Silverstein, S. D., & Mathews, C. P. (1993b). Beamspace root-MUSIC for minimum redundancy linear arrays. *IEEE Transactions Signal Processing*, 41, 2502–2507.